Bernardo Noiva Raposo Fernandes de Melo

Licenciado em Engenharia de Micro e Nanotecnologias

Chitin nanocrystals-alginate bioinks for bioprinting of 3D structures

Dissertação para obtenção do Grau de Mestre em

Engenharia de Micro e Nanotecnologias

Orientador: Doutora Susete Fernandes, Investigadora Doutorada, CENIMAT/I3N-Departamento de Ciência dos Materiais, Faculdade de Ciências e Tecnologia da Universidade Nova de Lisboa

Co-orientador: Professor Doutor João Paulo Borges, Professor Associado com Agregação, Departamento de Ciências dos Materiais, Faculdade de Ciências e Tecnologia da Universidade Nova de Lisboa

FACULDADE DE CIÊNCIAS E TECNOLOGIA
UNIVERSIDADE NOVA DE LISBOA

Abril 2019

Chitin nanocrystals-alginate bio-inks for bio-printing of 3D structures

Acknowledgments

Em primeiro lugar gostaria de agradecer à Universidade Nova de Lisboa, à Faculdade de Ciências e Tecnologia da Universidade Nova de Lisboa, ao Departamento de Ciências dos Materiais e ao CENIMAT por me acolherem e fazerem sentir em casa ao longo destes anos de licenciatura e mestrado.`

À doutora Susete Fernandes, a minha orientadora, por toda a paciência e disponibilidade que sempre demonstrou por todo o conhecimento transmitido ao longo do desta jornada. Ao professor doutor João Paulo Borges, o meu co-orientador, por ter feito crescer em mim a paixão por biomateriais. Ao Diogo Saraiva por toda ajuda no laboratório, à Ana Gaspar e à professora Isabel Ferreira pelo apoio na impressão 3D, ao Henrique Carrêlo e à professora Teresa Cidade pelo apoio nos testes reológicos. A todas as pessoas do laboratório 107 que de alguma forma me ajudaram e me tornaram um bocadinho mais independente dentro do laboratório.

À anTUNiA, por todas as histórias "para não contar aos netos" que passei e que ainda estão para vir. Um especial obrigado ao Bocage, ao Bolo-Rei, ao Bujão, ao Miúdo-Novo e ao Pau, vocês são lendários.

À minha namorada Filipa por tudo e mais ainda, sou o maior sortudo.

Por fim, os maiores agradecimentos são especialmente para os meus pais e para a minha irmã, mas também para toda a família, pelo apoio incondicional ao longo de todos estes anos.

Obrigadão.

Este trabalho foi financiado utilizando fundos concedidos pela FEDER através do Programa COMPETE 2020 e Fundos Nacionais, através da FCT – Fundação para a Ciência e Tecnologia e também POR Lisboa2020 ao abrigo do projeto POCI – 01-0145-FEDER-007688 (Referenciar UID/CTM/50025), e PTDC/CTM-REF/30529/2017 (NanoCell2SEC), e através de M-ERA.NET através do projeto M-ERA-NET2/0007/2016 (CellColor).

"Hard Work Pays Off"

by Mathew Fraser

Resumo

Bioimpressão é uma tecnologia de impressão onde um modelo tridimensional (3D) é construído por deposição sucessiva de camadas de biomateriais com células viáveis incorporadas, permitindo a produção de células, tecidos ou órgãos. Biocompatibilidade, biodegradabilidade, bons mecanismos de reticulação, propriedades reologias apropriadas e capacidade de impressão são as características mais importantes de uma biotinta, tipicamente obtidas de hidrogéis poliméricos.

Os hidrogéis de alginato têm sido muito usados em aplicações de bioimpressão porque são de fácil reticulação, baixo custo, abundantemente disponíveis e apresentam boa biocompatibilidade. No entanto, as soluções precursoras geralmente apresentam baixa viscosidade e comportamento de fluxo newtoniano a baixas taxas de cisalhamento (viscosidade de cisalhamento zero), o que pode levar à deformação das construções a imprimir após a deposição da solução precursora pela agulha no processo de extrusão. Este comportamento pode ser superado pela adição de modificadores de viscosidade, como a nanocelulose e a nanoquitina, que aumentarão a viscosidade das soluções precursoras e lhes darão uma viscosidade de cisalhamento diferente de zero a baixas taxas de cisalhamento. O objetivo principal desta dissertação é a produção e caracterização de hidrogéis compostos por alginato e nanocelulose ou nanowhiskers de quitina e avaliar sua capacidade de impressão 3D como biotintas.

A nanocelulose foi obtida com sucesso a partir de hidrólise ácida e foi preparada como solução aquosa com uma concentração de 1,9 % p/p. Adicionalmente, os nanowhiskers de quitina foram também obtidos com sucesso a partir de hidrólise ácida e duas soluções aquosas foram preparadas a 1,9 % p/p e 2,7 % p/p. As soluções aquosas foram posteriormente misturadas com alginato em diferentes proporções, a fim de estudar o mecanismo de reticulação das biotintas.

As estruturas 3D foram impressas usando uma técnica de impressão manual 3D e uma técnica de impressão 3D utilizando as biotintas e as soluções de reticulação. Este trabalho mostra o progresso das condições de impressão até a obtenção de estruturas impressas com sucesso, utilizando hidrogéis e recursos naturais como celulose e quitina.

Palavras-chave: bioimpressão, biocompatibilidade, nanocelulose, nanoquitina, alginato, reticulação, impressão 3D.

Abstract

Bioprinting is a 3D printing technology to deposit layer-by-layer stacking patterns of biomaterials with incorporated viable cells, enabling the production of cells, tissues or organs. Biocompatibility, biodegradability, good cross-linking mechanisms, good rheological and printability are the most important features of a bioink which are typically achieved with polymer hydrogels.

Alginate hydrogels have been found much use in bioprinting applications because they are so easily cross-linked, low cost, abundantly available, and have shown good biocompatibility. However, their gel precursor solutions generally present low viscosity and Newtonian flow behavior at low shear-rates (zero shear viscosity), which can lead to deformation of printed constructs after deposition from the needle in the extrusion printing process. These mechanical problems can be overcome adding viscosity modifiers such as nanocellulose and chitin, that will enhance the viscosity of the precursor solutions and will give them a yield point at low shear rates rather than a zero. The main goal of this dissertation is the production and characterization of hydrogels composed by alginate and nanocellulose or chitin nanowhiskers and evaluate its 3D printability as bioinks.

Nanocellulose was successfully obtained from acid hydrolysis and was prepared as a aqueous solution with a concentration of 1.9 % wt.. Additionally, chitin nanowhiskers were also successfully obtained from acid hydrolysis and two aqueous solutions were prepared at 1.9 % wt. and 2.7 % wt.. The aqueous solutions were posteriorly mixed with alginate at different proportions in order to study the cross-linking mechanism of the bioinks.

3D structures were printed using “hand-draw” 3D printing and 3D printing techniques resorting the bioinks and cross-linking solutions. This work shows the progress of the printing conditions until successfully printed structures were obtained, using hydrogels and natural resources like cellulose and chitin

Keywords: bioprinting, biocompatibility, nanocellulose, nanochitin, alginate, cross-linking, 3D printing

Table of contents

List of figures

List of tables

Acronyms

3D	3 Dimensional
AFM	Atomic Force Microscopy
ATR	Attenuated Total Reflectance
CMC	Cellulose Microcrystalline
CNC	Cellulose Nanocrystal
CTNW	Chitin Nanowiskers
d	Diameter
$\mathbf{d_r}$	Diameter of each rod
DD	Degree of Deacetylation
DSC	Differential Scanning Calorimetry
FTIR	Fourrier-Transform Infrared
$\mathbf{I_C}$	Cristallynity Index
L	Length
$\mathbf{L_r}$	Length of each rod
M	Molecular weight
$\mathbf{\bar{M}}$	Average molecular weight
PVA	Polyvinyl Alcohol
RH	Relative Humidity
TGA	Thermogravimetric Analysis
XRD	X-Ray Diffraction

1 Introduction

1.1 Tissue engineering and bioprinting

In 1987, Robert S. Langer introduced to the world the term “tissue engineering”, result of the work of several generations of marine and development biologists studying cell and tissue coalescence phenomena, cell adhesion and tissue biocompatibility. Their concerns were focused on developing methods to enhance the regenerative properties of tissues involved in the healing [1]. Therefore, the main goals of tissue engineering start to be the understanding of the mechanisms that control and contribute to tissue organization and development of materials able to improve the functions of a tissue in an organism, or even, replace it wholly or partially [2].

It is known that the existing supply of functional tissues and solid-organs is far from the demand on the transplants waiting lists. Most of the times, suitable tissues are either obtained from the patient (autografts) or from tissue banks (allografts) to be used for healing or replacement of tissues damaged by burns or repairing bone and dental defects. However, sometimes the sources are insufficient for use in traumatic injuries where a significant quantity of tissue replacing is needed such as motor vehicle accidents, war injuries or extensive burns. Furthermore, poor life quality issues can arise due loss of motor control or lack of sensitivity due to nerve damage after tissue transplanting. Even though we are decades away from being capable to fabricate in the laboratory an anatomically sized complex organ such as kidney, liver or heart, great progress has been reported in the engineering of small-volume tissues and multi-tissue constructs over the past decade. The investment on the technology’s development of the manufacture of transplantable tissues and functional organs can lead to a reduction and an utopic elimination of the organ waiting list [3].

One of the most potential technologies for engineering new tissues and organs is bioprinting. Bioprinting is a 3D printing technology to deposit layer-by-layer stacking patterns of bioinks constituted of biomaterials that might incorporate viable cells, enabling the production of cells, tissues or organs. This technology has been in the spotlight of several researchers and has received immense consideration due to its large application spectrum (regenerative medicine, tissue engineering, transplantation, drug delivery, etc.) and equally wide list of advantages, such as high precision and control over construct geometry, composition, configuration and high level of customization [3, 4].

Different fabrication strategies are being used to fabricate biomaterials including molding, blending, microfluidic techniques, magnetic assembly and even more. On the other hand, bioprinting is a manufacturing technology that can reach high level of tissue construct accuracy, with porous structures, controlled architecture and with high-throughput fashion. Additionally, bioprinting allows

the co-culturing of multiple cell types within a structure, and facilitate controlled delivery of drugs, genes, and growth factors [5]. The elimination of the 'human element' through the use of a 3D printer conducts to the reduction of the error and enhance the consistency and the repeatability of the fabricated structures [3].

To date, several 3D printing techniques have been developed but only few are suitable to bioprinting due to lack of resolution, type of materials used or other features. The three major techniques used for bioprinting are inkjet, laser-assisted, and extrusion bioprinting, and, as described by Mandrycky *et al.* [6], each has specific strengths, weaknesses and limitations. Although none of the bioprinting techniques have enabled the production of complex tissues at all scales, many researchers are attempting to model the diverse parameters of the printers such as dispensing pressure, nozzle diameter, printing time or substrate used, and refine the bioinks features.

1.2 Bioinks

Bioinks used to produce scaffolds (printed structures) to replace and/or repair damaged tissues must meet several criteria to be considered suitable for clinical applications, especially biocompatibility. Biocompatibility refers to the ability of a material to interconnect with the host and without harm, perform its purposes correctly. For *in vivo* applications, biodegradability also plays a very important role because when hosted, the material can be degraded or integrated with the extracellular matrix of cells, and it is crucial that its degradation occurs without generating harmful products or have establishment of negative interactions with cells [6]. These are the two most obvious features, but proper mechanical, rheological and printable characteristics are equally important. A printable bioink may exhibit a fast response to re-establish the high zero-shear viscosity after extrusion, must withstand forces applied during the printing process, presents good cross-linking mechanisms and high post-printing structural fidelity. Its porosity and morphology are very important which refers to the transfer and movement of nutrients and oxygen through the engineered complex and must enable the attachment of cells, and encourage cellular proliferation and differentiation to promote bioactivity [7, 8]. Some of the desired characteristic of a bioink can be achieved with polymer hydrogels.

Hydrogels can be described as a group of polymeric materials, which have a hydrophilic polymeric network with high flexibility and high capacity to retain water. There are two categories of hydrogels based on the type of cross-linking. Chemically cross-linked hydrogels where the networks have permanent bonds, and physical cross-linked that arise from either interconnections between polymeric chains or physical interactions such as ionic interactions or hydrogen bonds [9]. Hydrogels can be obtained from natural or synthetic sources, and they are of interest because of their structural similarity to cell's extracellular matrix. In tissue engineering, hydrogels have been used as a medium to pattern

cells in a three-dimensional space during and after bio fabrication. Because of its role as provisional extracellular matrices, the majority of hydrogels on the market are from natural sources, including collagen (type I), gelatin, fibrin, hyaluronic acid, agarose and alginate [10].

Alginate hydrogels have been found much use in bioprinting applications because they are so easily cross-linked. They are abundantly available, present a low cost, and have shown good biocompatibility with negligible inflammatory effect after *in vivo* implantation. The ability to easily tune the viscosity by modifying the concentration of precursor solution and degree of cross-linking before and after deposition, makes this type of hydrogels very versatile in terms of processing and mechanical characteristics for bioprinting applications [10]. However, their gel precursor solutions generally present low viscosity and Newtonian flow behavior at low shear-rates (zero shear viscosity), which can lead to deformation of printed constructs after deposition from the needle in the extrusion printing process. These mechanical problems can be overcome adding viscosity modifiers such as nanocellulose and chitin, that will enhance the viscosity of the precursor solutions and will give them a yield point at low shear rates rather than zero [11, 12].

1.3 Cellulose and its derivates

Cellulose is the most abundant biopolymer available on Earth, and it can be obtained from several sources such as plants, bacteria, fungi or marine animals. As a natural polymer, cellulose is composed of D-glucopyranose units which are linked together by β-1,4 glycosidic bonds, whose repeat segment is usually considered a dimer of glucose called "cellobiose". In nature, cellulose exists, for instance, in the plants cell wall, as a linear crystalline macromolecule (polysaccharide) of high molecular weight and high degree of polymerization.

When chains of macromolecular cellulose aggregates parallelly and establish intermolecular hydrogen bonds, it forms microfibrils of varying dimensions with crystalline regions. The hydrogen bonding between surface hydrogen and oxygen molecules, intra and inter cellulose chains in the crystalline regions is believed to be responsible for the anisotropy of the elastic properties of cellulose, where Young's Modulus and Poisson's ratio exhibit crystallographic dependence. However, when the cellulose chains are not parallel to each other, some amorphous regions can occur (Figure 1.1 b) [13].

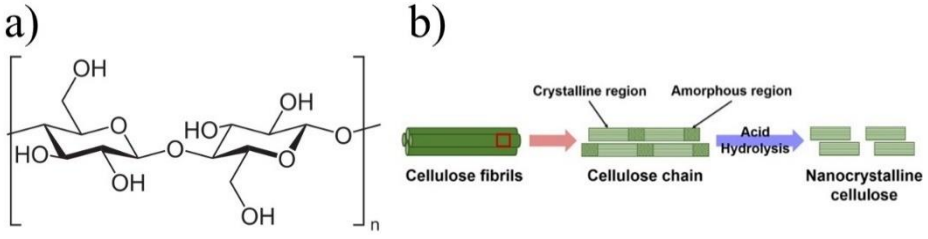

Figure 1.1 – a) Schematic representation of the chemical structure of cellobiose which is the repeating unit of cellulose. Cellobiose is divided into two anhydroglucopyranose units, connected by a β-1,4 linkage. b) Illustrations of a cellulose fibril divided into crystalline and amorphous regions, and the acid hydrolisis reaction to obtain nanocrystalline cellulose. Images adapted from [14, 15]

The isolation of the crystallites can yield individual elements such as cellulose microcrystalline (CMC) or cellulose nanocrystalline (CNC). Both CMC and CNC are obtained from acid hydrolysis (Figure 1.1 b); however, different processing features lead up to different products. On a previous study by Araki *et al.* [16], it is described that CNCs prepared by sulfuric acid hydrolysis form more stable suspensions than those obtained by hydrochloric acid hydrolysis, because the former produces negatively charged crystallites through the sulfate esters introduced during hydrolysis, thus preventing the NCC particles to aggregate and allow the formation of stable colloidal suspensions in water. Characteristics such as large and highly reactive surface, high specific strength and Young's modulus and low density, makes CNCs a strong biomaterial to use as rheological modifier, nucleating agent, or a high-performance scaffold in polymers, gels, hydrogels and emulsions. Additionally, CNCs can be obtained from theoretically unlimited sources which makes it a very interesting nanomaterial for production of low-cost, lightweight, strong and renewable nanocomposites [13, 17].

1.4 Chitin and its derivates

Chitin, poly (β-(1,4)-N-acetyl-D-glucosamine), is a natural polysaccharide synthesized by a large group of living organisms, and it is considered the second most abundant polymer on the planet, right after cellulose (Figure 1.2). In chitin, the fraction of N-glucosamine units is defined as the degree of the deacetylation (DA), and it is lower than 0.5 (typically between 0.1-0.3). When the N-glucosamine units are predominant (DA > 0.5), the biopolymer is designated chitosan, the most important derivative of chitin [18].

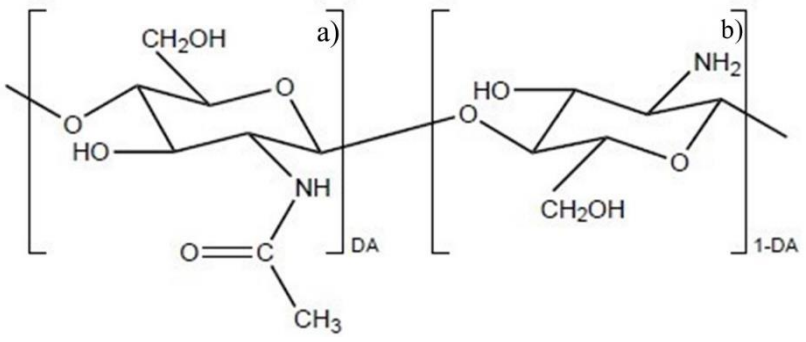

Figure 1.2 – Schematic representatino of the chitosan/chitin molecule. a) N-acetylglucosamine unit; b) N-glucosamine unit. When DA is higher than 0.5 chitin is obtained. Chitosan obtained when 1-DA is higher than 0.5. Image adapted from [19].

Chitin occurs in nature as structural component in the exoskeleton of all arthropods (insects, arachnids and crustaceous), in the cell walls of fungi and green algae, and in the shell of molluscs. Depending on its source, chitin can be classified into α, β or γ forms. α-chitin is the most abundant form and its highly ordered crystalline structure that results from the large number of intra- and inter-molecular hydrogen bonds. In the α form, polymeric chains are packed anti-parallel, which allows the inter-molecular bonding, conferring the biopolymer interesting rigid properties. On the other hand, β-chitin chains are stacked in a parallel disposition, which does not favour inter-molecular bonding and makes β-form more soluble in water then α-form. The third form, results from the combination of α and β-chitin, with a three-chain unit structure where two chains are parallel and the third one is in an anti-parallel arrangement [18, 20].

Generally, the aggregates of chitin's consecutive units lead to the formation of highly crystalline fibrils often denominated chitin nanocrystals or chitin nanowhiskers (CTNW). These nanowhiskers, among other methods, can be obtained by acid hydrolysis of chitin. Alongside with chitosan derivatives, the nanowhiskers are recognized by the scientific community as biomaterials that possess unique features such as biodegradability, bioactivity, non-toxicity, antibacterial, antifungal and anti-inflammatory activity, capacity to accelerate wound-healing and act as reinforcement in nanocomposites. Areas such as pharmaceutics, cosmetics, agriculture, biosensors, water treatment and tissue engineering have given lot of attention to this polymer [18, 20, 21].

This dissertation was based on the work that has been being developed by Paul Gatenholm and his study group, which have been focusing on cartilage tissue engineering using a bioprinting method of nanocellulose and alginate bioinks. The Figure 1.3 presents a miniature ear constructed by Muller *et al.* [11]. Their works served as the basis for the formulation of the inks as well as characterization and printing methods [11, 22].

Liu, et. al [23], recently published a review about current advances and future perspectives of bioinks made by natural-derived polymers to 3D printing. In this paper it is described the state-of-the-art referring to bioinks made by natural-delivered polymers such as cellulose-based materials, some of them with alginate (Markstedt *et al.* [24], Martinez Ávila *et al.* [25]); starch-based materials; algae-based materials; and chitosan-based biomaterials (Almeida *et al.* [26], Demirtaş *et al.* [27], Foresti *et al.* [28]). However, to the best of our knowledge, a bioink made by chitin nanowhiskers and alginate has never been studied or developed. This dissertation's main goal is to develop a bioink composed by chitin nanocrystals and alginate, in order to print 3D structures

Figure 1.3 - 3D printed ear using a bioink composed by alginate sulfate and nanocellulose. Scale bar: 5 mm. Image adapted from [11].

2 Materials and Methods

2.1 Cellulose nanocrystals production

Microcrystalline cellulose (10 g, Avicel® PH-101, particle size ≈ 50 μm, lot# BCBP6787V) derived from cotton as indicated by the supplier, Sigma-Aldrich and sulphuric acid (95 % to 97 % purity and M=98.08 g/mol) GPR RECTAPUR® purchased from VWR Chemicals, were used without additional treatment.

Cellulose nanocrystals preparation was based on a previous study described by Fernandes *et al* [29], starting with the acid hydrolysis of microcrystalline cellulose with an acid/solid ratio of 8.5:1, at 45 ºC, during 130 minutes under vigorous stirring and quenched with ultrapure water (collected from Millipore Elix Advantage 3 system). After removing the supernatant, the resulting material was centrifuged for 20 minutes at 20,000 rpm, for consecutive cycles with ultrapure water. The CNCs' collected suspension, presented a pH between 1.9 and 3.9 and was posteriorly purified by dialysis against ultrapure water for a minimum of 15 days. The CNC suspension with 3.60 ± 0.02 % (w/w) (gravimetrically determined) was sonicated and used in its acid form (pH = 3.5).

2.2 Chitin Nanowhiskers production

Chitin (10 g, coarse flakes, lot# SLBB 8542V) derived from shrimp shells as indicated by the supplier, Sigma Aldrich and hydrochloric acid (37 % purity and M=36.461 g/mol) from Carlo Erba Reagents, were used without additional treatment.

Chitin nanowhiskers was produced following the method described on João *et al.* [19]. Initially 10 g of chitin were hydrolyzed with a 100 mL HCl 3M solution at 110 ºC, during 90 minutes under vigorous stirring and quenched with ultrapure water. When precipitated, supernatant was removed, and the resulting material centrifuged with 15 minutes cycles at 11,000 rpm, adding ultrapure water until pH = 2. Final chitin suspensions were kept and dialyzed against ultrapure water until a constant pH was achieved, and finally freeze-dried for 24 hours.

2.3 Bioinks preparation

Alginic Acid Sodium Salt ($\overline{M}$=10,000 – 600,000 g/mol, lot#6A012793) from BioChemica and d-manitol (98 % purity, M=182.17 g/mol, lot#BC8V1712) purchased from Sigma Aldrich were used as received.

The bioinks preparation was based on the previous study described by Muller *et al.* [11] although some adaptations were necessary. A solution of alginate at 3 % (w/w) in a 4.6 % (w/v) aqueous solution of d-mannitol was prepared, as well as, aqueous suspensions of cellulose nanocrystals (CNCs) at 1.9 % (w/w) and chitin nanowhiskers (CTNW) at 1.9 % (w/w) and 2.7 % (w/w). 100 mL of CNC:alginate inks with volume/ratio of 4.2:1 and CTNW:alginate inks at 4.2:1, 4:1, 3.5:1, 3:1 and 2.5:1 volume/ratio were prepared.

2.4 "Hand-draw 3D printing"

Poly (vinyl alcohol) (95 %, M.W.=95,000) acquired from Acros Orgarnics, Calcium chloride-dihydrate ($CaCl_2.H_2O$, M=147.02 g/mol, 99 % purity) purchased from Carl Roth, Polystyrene Petri Dish (diameter=35 mm), TE Dispensing Tip (Gauge 20, inner diameter 0.02375 mm, outer diameter 0.918 mm, TE720150), disposable syringe (B Braun, 1 mL).

The cross-linking solutions were prepared by dissolving calcium chloride dihydrated ($CaCl_2.2H_2O$) in ultrapure water and in PVA at different concentrations as presented in Table 2.1.

The cross-linking solution was added to a Petri dish containing a paper substrate. Posteriorly, a system consisting of a syringe containing the ink suspension and a needle immersed on the cross-linking solution and the printing was handmade. A qualitative assessment of the gelation process was done at specific times (after 20, 30 and 60 minutes) where a spatula was used to test the robustness of the structure. After the cross-linking process, the structures were removed from the cross-linking solution, washed softly against ultrapure water, dried with filter paper and finally kept at a 4 ºC controlled environment (RH=72 %).

Table 2.1 – Concentrations of cross-linking solutions.

PVA (% wt.)	**$CaCl_2$ (mM)**
0	100
5	100
10	25
	50
	100

2.5 3D printing

The designing of the structures was made at Tinkercad™, which is an online software tool. From this tool we extracted the .STL files that were posteriorly converted in G programming language (G-code) to be read directly by the printer. A preview of the structures is presented in supplementary information in Figure 6.5.

The printing process, performed by a homemade adapted printer, was done over a glass substrate, spraying the cross-linking solution over the formed structure at a room temperature of 22 ºC and relative humidity of 54 %. For the cross-linking process a $CaCl_2$ 100 mM aqueous solution was used. The bioinks CNC (1.9 % wt.):alginate,CTNW (1.9 % wt.):alginate and CTNW (2.7 % wt.):alginate used for printing were 4.2:1. 4:1 and 4:1 volume ratio respectively. After the printing process, the structures were removed from the glass substrate, washed softly against ultrapure water, dried with filter paper and finally kept at a 4 ºC controlled environment (RH = 72 %).

2.6 Characterization

2.6.1 Chemical, Structural and dimensional characterization

Elemental analysis, Fourier-transformed infrared (FTIR), scanning calorimetry with thermogravimetric analysis (DSC-TG), x-ray diffraction (XRD), dimensional measuring resorting to atomic force microscopy (AFM) images were made for samples of CMC, CNC, chitin and CTNW. Standard parameters were used, and can be found, along with the equipment used, in the supplied supplementary information in section 6.1.

2.6.2 Rheological characterization and Swelling behavior

Rheological characterizations were made to the CNC:alginate and CTNW:alginate at different cross-linking solutions and the standard parameters used can be found, along with the equipment used, in the supplied supplementary information in section 6.2.

Swelling tests were performed on the CNC:alginate and on CTNW:alginate hydrogels and the technique used is presented in section 6.2.

3 Results and discussion

This dissertation's main goal was the production and characterization of hydrogels based on alginate and nanochitin and evaluate its 3D printability as bioinks.

The first part of this work focused on the synthesis of cellulose and chitin nanocrystals obtained from microcrystalline cellulose and shrimp shells, respectively. Thereafter, chemical, structural, dimensional and mechanical characterizations were performed on the raw material, its nanocrystals and on the hydrogels prepared from alginate solutions. It is important to note that CNCs/alginate hydrogels were prepared to be used as a model based on a similar work presented by Muller *et al.* [11]. "Hand-draw 3D printing" technique was used and optimized in order to qualitatively evaluate the robustness of hydrogels obtained at several conditions. Finally, it was possible to print the bioinks using a homemade 3D printer as a proof-of-concept.

To facilitate the presentation and discussion of hydrogels' preparation and characterization, all the results are presented together.

3.1 Cellulose and chitin derivates characterization

The chemical analysis of microcrystalline cellulose, cellulose nanocrystals, chitin and chitin nanowhiskers was done by ATR-FTIR and the spectra are presented in Figure 3.1 and Figure 3.2.

In both spectra presented in Figure 3.1, it is possible to identify all the characteristic IR absorption frequencies attributed to the functional groups of cellulose. The stretching vibration of the O-H bond can be found at 3,330 cm^{-1}, the C-H stretching at 2,899 cm^{-1} and the C-O stretching at 1,030 cm^{-1}. Due to the presence of sulfate groups on the CNC sample added by the hydrolysis process, a peak assigned to S-O bonds stretching can be detected on this sample at 812 cm^{-1}. All assignments are in agreement with the observed values found in the relevant literature [30].

The same way, in Figure 3.2 it is possible to identify the major α-chitin characteristic bands. The absorbance region observed around 3,430 cm^{-1} its attributed to the stretching vibration of O-H bonds stretching; the bands at 1,654 cm^{-1} and 1,618 cm^{-1} are attributed to the carboxyl groups (C=O) vibrations of amide bonds. The presence of amide is strengthened by the appearance of C-N absorption band at 1,375 cm^{-1} and N-H bending at 739 cm^{-1}. Meanwhile, the bending vibration of C-O bond is present at 1,006 cm^{-1}. Chitin's anomeric center (C1) vibration can be attributed to the 893 cm^{-1} peak, a typical band that appears in chitin from shrimp. The FTIR spectra revealed good correspondence with values reported in the literature, with a slight shift of the peaks to the left (higher wavenumbers) [18, 31].

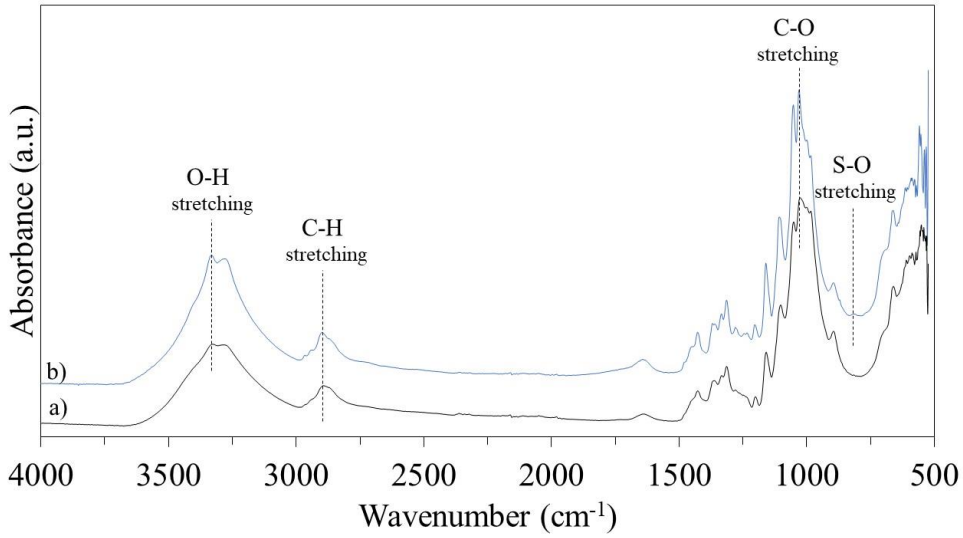

Figure 3.1 - FTIR spectra of a) CMC and b) CNC.

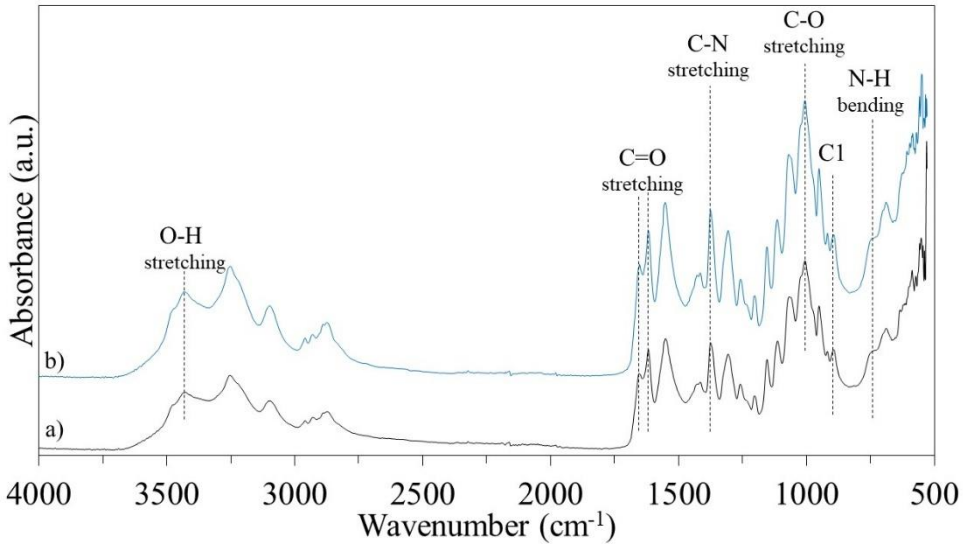

Figure 3.2 - FTIR spectra of a) Chitin and b) CTNW.

Structural and morphological characterization are also a very important type of characterization to access the effect of the acid hydrolyses reaction on CMC and chitin with sulfuric acid and hydrochloric acid respectively , so XRD and AFM were performed in order to confirm the successful production of cellulose nanocrystals and chitin nanowhiskers.

XR diffraction patterns are presented in Figure 3.3 and Figure 3.4 where a comparison is made between the starting materials and the nanostructures obtained from acid hydrolysis. Observation of

the diffraction patterns in Figure 3.3, clearly show the characteristic peaks of cellulose Iβ polymorph on both samples, with the (002) plane peak centered at 22.6 º, the (101) peak at 15.4 º, and finally the (040) contribution at 34.7 º, maintaining the same pattern across both samples and confirming the stability of the cellulose structure after acid hydrolysis [32].

The Figure 3.4 shows the diffraction patterns of the chitin prior to hydrolysis and the chitin nanocrystals. The diffraction patterns for both materials show typical peaks of pure α-chitin, indicating that the crystal integrity was maintained after the hydrolysis process. The five more intense peaks are located at 9.4 º, 12.7 º, 19.4 º, 23.5 º and 26.5 º and are indexed as the 020, 101, 110, 130 and 013 reflections according to the structure of α-chitin [19].

The crystallinity index (I_C) was determined by using the documented empirical method described at Segal *et al.* [33] and Clark *et al.* [34]. The data extracted from Figure 3.3 and Figure 3.4 was used in the following equation:

$$I_C = \frac{I_{max} - I_{am}}{I_{max}} \times 100$$

where, I_{max} is the maximum diffraction intensity of (002) lattice peak for the cellulose samples and (110) lattice peak for the chitin samples. For cellulose samples, the (002) lattice peak was at a 2θ angle between 22 º and 23 º; while for chitin samples, the (110) lattice peak was at a 2θ angle between 19 º and 20 º. I_{am} is the intensity of the amorphous material. For cellulose samples, was considered the region of 2θ angle between 18 º and 20 º; while for chitin samples, was considered the region of 2θ angle between 10 º and 13 º, and the I_{am} was the lowest intensity value inside the considered range. This calculation method is only valid as a comparison basis between samples.

A summary of the results obtained is presented in Table 3.1. The values obtained are in accordance with reported values available in literature [30].

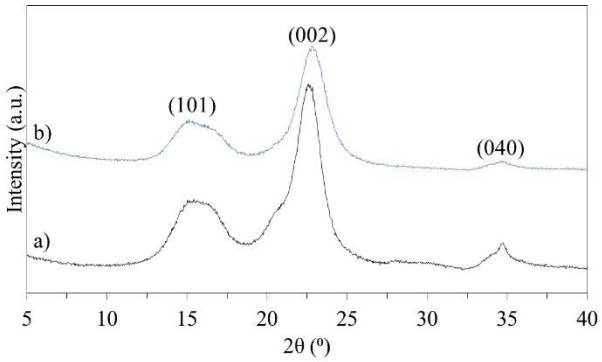

Figure 3.3 – XRD diffraction patterns of a) CMC and b) CNC.

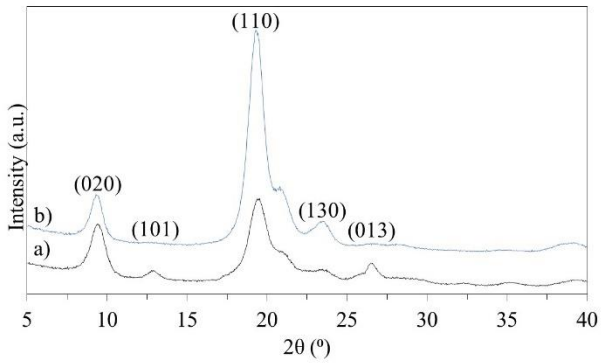

Figure 3.4 - XRD diffraction patterns of a) Chitin and b) CTNW.

Table 3.1 - Relative Cristallinity Index measurements obtained by the Segal and Clark methods for cellulose micro- and nanocrystalline, chitin and chitin nanowiskers samples.

Sample	I_{max}	I_{am}	I_C (%)
CMC	13,105 (at 22.6 º)	3,011 (at 18.8 º)	77
CNC	8,482 (at 22.8 º)	1,594 (at 18.8 º)	81
Chitin	8,003 (at 19.5 º)	1,349 (at 11.6 º)	83
CTNW	19,043 (at 19.3 º)	1,204 (at 11.9 º)	94

Atomic Force Microscopy was posteriorly used to dimensionally characterize the CNC and CTNW samples and validate the production of nanowiskers. Figure 3.5, below, shows AFM captured topographic images of both CNC and CTNW dispersed samples. The samples were equally prepared from a 0.01 % (w/w) aqueous suspensions, and after dried, a rod-like shape nanoparticles can be observed in both samples.

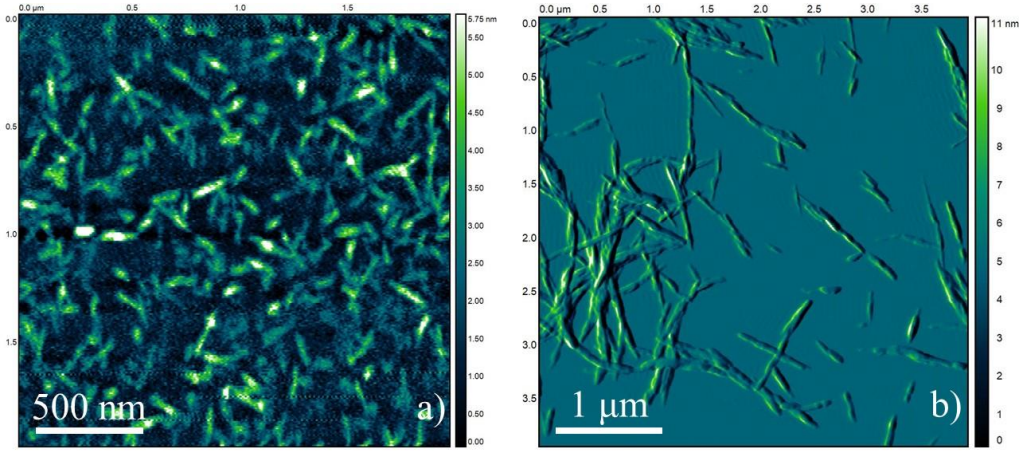

Figure 3.5 – AFM captured images, in amplitude retrace mode. a) CNC rods; b) CTNW.

CNC particles dimensions were obtained from 159 individual rod measurements on the images obtained by AFM and calculated to be, on average 135 ± 48 nm of length (*L*) and 4 ± 1 nm of diameter (*d*). These values equate to an approximate aspect ratio (*L/d*) of 38:1. The average measured length of the particles is in accordance with literature as reported by Fernandes *et al.* [29] (under similar hydrolysis conditions). Nonetheless, these results confirm that nanoparticles are obtained by the acid hydrolysis of microcrystalline cellulose (with average dimensions of ~50 µm as reported by the supplier).

In order to determine the CTNW dimensions, several images obtained by AFM were used to measure a total of 109 individual rods. On average, the dimensions length, diameter and aspect ratio (*L*/d) were calculated to be 344 ± 127 nm, 6 ± 1 nm and 54:1, respectively. While the average measured length of the particles is in accordance with literature as reported by João *et al.* [19] (under similar hydrolysis conditions), the determined diameter is lightly smaller.

The method used to determine the dimensions of the nanoparticles was a method described in the literature by Honorato-Rios *et al.* [35]. This method is very precise because the determination of the diameter of each rod is done by averaging the diameter through its length, and not by measuring its width, and it is extensively described in Supporting Information.

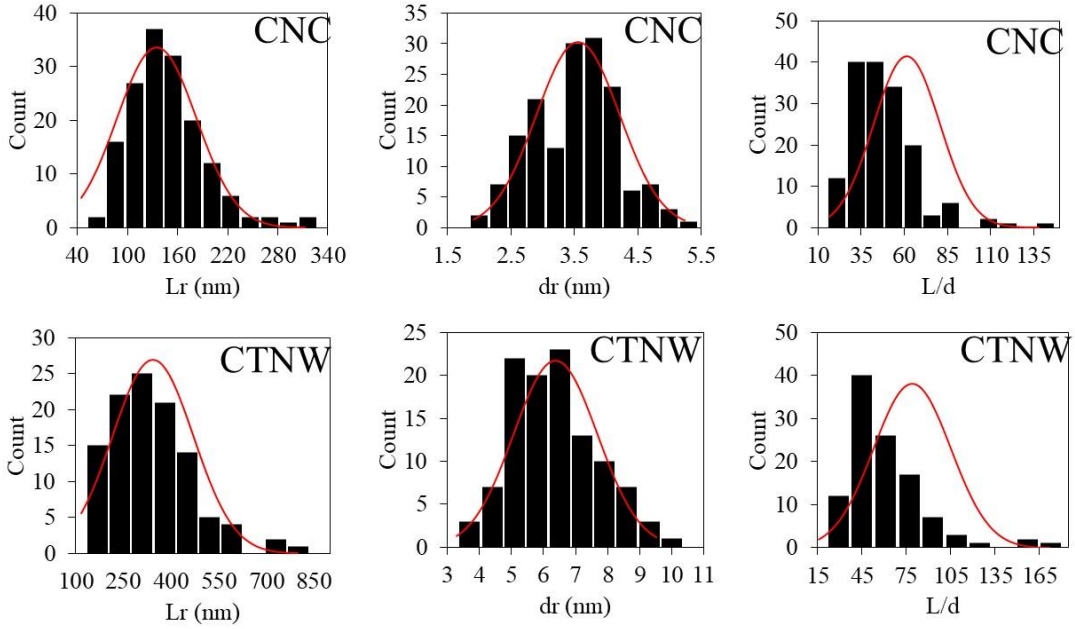

Figure 3.6 - Distributions of the measures determined using AFM of both CNC and CTNW samples. From left to right length (*L*), diameter (*d*) and aspect ratio (*L/d*) distributions respectively. *Lr* and *dr* refers to the length and diameter of each rod.

Figure 3.7 and Figure 3.8 show the thermogravimetric and DSC curves (along with respective TGA curves) of cellulose microcrystalline, cellulose nanocrystals, chitin and chitin nanowhiskers and allow to determine the thermal stability of the produced nanomaterials.

The CMCs' TG curve presents the typical first-order reaction pyrolysis process of the cellulose as reported by Atalla *et al.* [36]. The CNC's TG curve can be divided into two main phases, the first weight loss between 50 ºC and 120 ºC that is attributed to loss of mass due to evaporation of residual water contained by the sample; the second, occurs between 220 ºC and 350 ºC, where diverse degradation processes take place such as decomposition, dehydration and depolymerization of glycoside units.

The CNC sample goes through this mass loss in two stages, since it experienced a hydrolysis process performed with H_2SO_4. The first stage (up to ~ 220 ºC) is associated with the degradation of regions more accessible to the sulphate groups, while the second one is attributed to the breakdown of the more crystalline regions of the sample, less affected by the hydrolysis process. On the other hand, the CMC's sample mass percentage takes an abrupt dive around 300 ºC. The final decrease from 350 ºC forward, is linked to the oxidation and breakdown of the samples' carbon-based residues [30, 32]. Similar curves have been previously obtained by *Martins et al.*[37].

Figure 3.8 shows TGA and DSC curves of chitin and CTNW samples where three characteristic temperature intervals of weight loss can be observed. The first, from 40 ºC to 300 ºC, where there was 5-10 % wt. weight loss due to the evaporation of hydrogen bonded water to chitin and CTNW

samples. The second weight losses, occurring between 300 ºC to 400 ºC, around 60 % wt. and is caused by decomposition/depolymerization of polymer chains through deacetylation and cleavage of glyosidic linkages. The third and final stage, for temperature value higher than 400 ºC, with a 10 % wt. weight loss, corresponds to the thermal destruction of pyranose ring and the decomposition of the residual carbon [38].

The thermal degradation of chitin takes place within 300 ºC and 460 ºC as it is presented in Figure 3.8 and as reported by Stawski *et al.* [39].

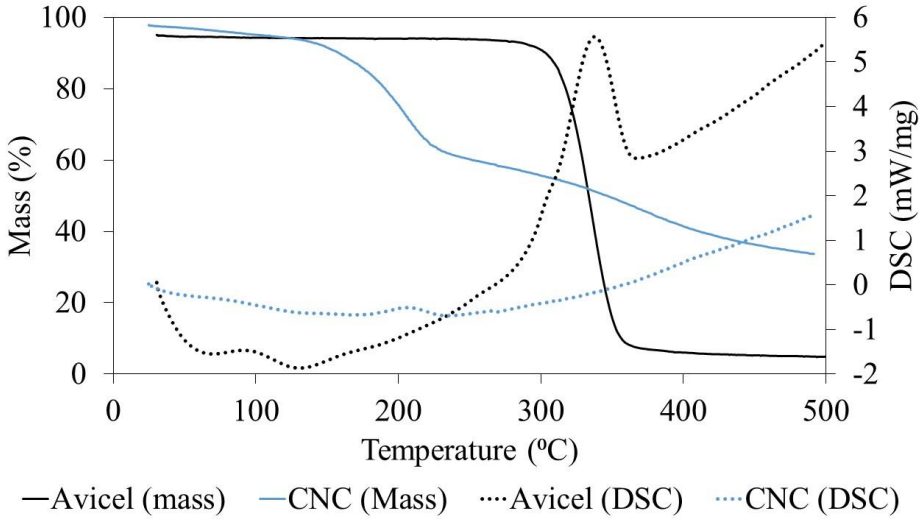

Figure 3.7 – Thermal analysis of microcrystalline cellulose (CMC) and nanocystalline cellulose (CNC) samples.

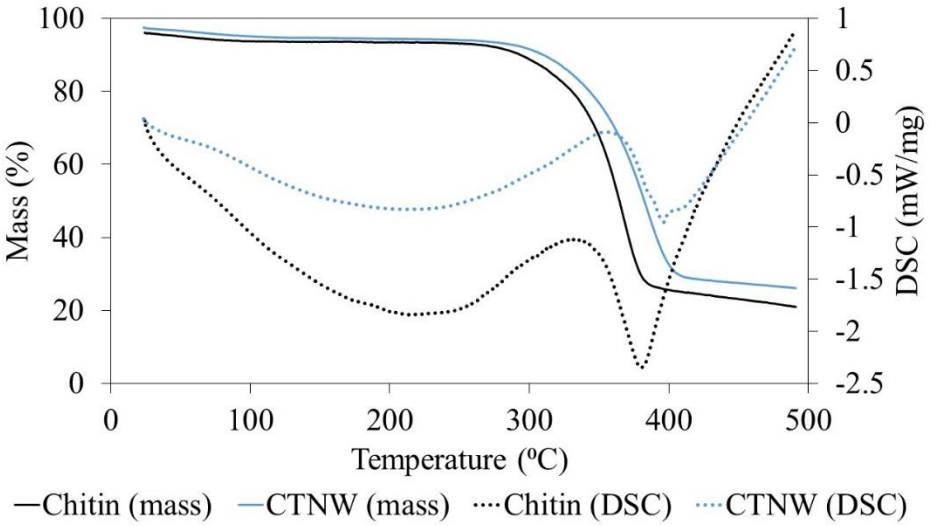

Figure 3.8 – Thermal gravimetic analysis of chitin and chitin nanowhiskers (CTNW) samples.

The rheological properties of alginate, CNC and CTNW suspensions, and formulated bioinks were determined resorting to a Bohlin Gemini HRnano rotational rheometer. These properties are very important to establish a relation between the shear-rate and the viscosity of the bioinks. Figure 3.9 and Figure 3.10 show the flow behavior of the materials as function of the shear-rate, which is very important to evaluate the viscosity of the materials at low shear-rates. In order to make a comparison between the CNC and the CTNW aqueous suspensions and the bioinks obtained, we started by testing the common denominator of the bioinks: the alginate solutions. The alginate presented a viscosity around 10 Pa.s for lower shear-rates, decreasing until 2 Pa.s at 100 s^{-1} of shear-rate. Posteriorly, the CNC and the CTNW aqueous solutions were evaluated, demonstrating a higher level of viscosity when comparing to alginate. At 0.01 s^{-1} shear-rate, the CNC and the CTNW (1.9 % wt.) aqueous solutions presented approximately 20 Pa.s and 100 Pa.s respectively and decreasing to around 0.1 Pa.s at 100 s^{-1} of shear-rate. These values of flow behavior are supported by previous studies as Bercea *et al.* [40] and W. Li *et al.*[41] respectively.

The bioinks CNC:alginate (4.2:1 volume ratio), CTNW (1.9 % wt.):alginate (4:1 volume ratio) and CTNW (2.7 % wt.):alginate (4:1 volume ratio) were also submitted to flow behavior experiment and, at low shear-rates, they presented 9 Pa.s, 10 Pa.s and 300 Pa.s of viscosity respectively. As described in the literature as by Muller *et al.* [11], alginate exhibit low viscosity and Newtonian flow behavior at low shear-rates, which can be overcome with the addition of viscosity modifiers like nanocellulose and chitin nanowhiskers. The values presented are in accordance with the literature since the bioinks with these nanoparticles present higher viscosity at lower shear-rates when comparing with alginate pristine solution. We also noticed that an increase on the concentration of CTNW in the bioink give rise to inks with higher viscosity (CTNW (1.9 % wt.):alginate (4.2:1 volume ratio): 10 Pa.s vs CTNW (2.7 % wt.):alginate (4:1 volume ratio): 300 Pa.s). This fact is only true when the concentration of chitin's suspensions is lower and bellow the liquid-crystal concentration because at this concentration the viscosity strongly decreases as described in W. Li *et al.* [41].

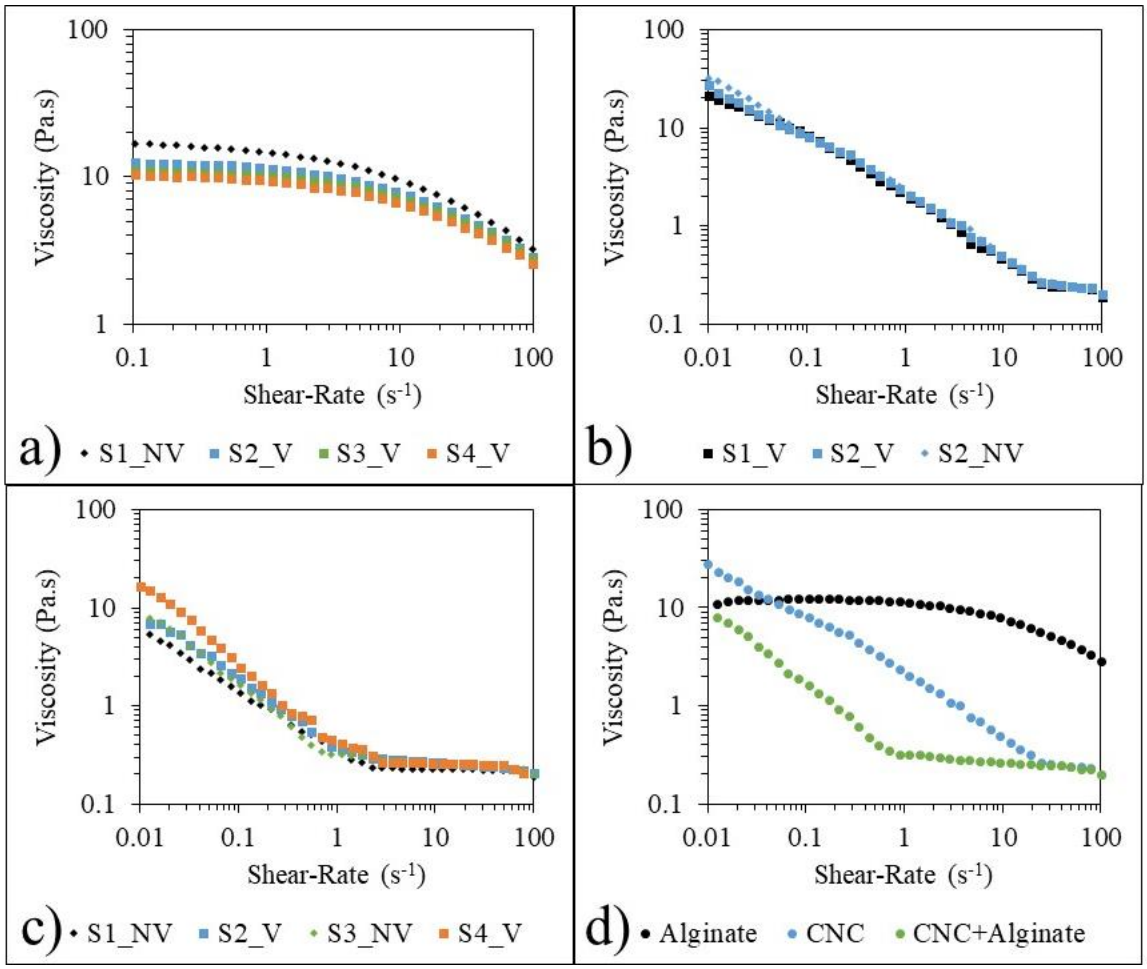

Figure 3.9 – Flow behaviour of: a) alginate samples; b) CNC (1.9 % wt.) samples suspensions; c) CNC (1.9 % wt.) with addition of alginate 4.2:1 volume ratio.d) Flow behaviour comparations between alginate and the CNC (1.9 % wt.) samples with (4.2:1 volume ratio) and without addition of alginate. S1, S2, S3 and S4 refers to the each sample used to the experiment, while V and NV indicates if the sample was virgin or non-virgin respectively.

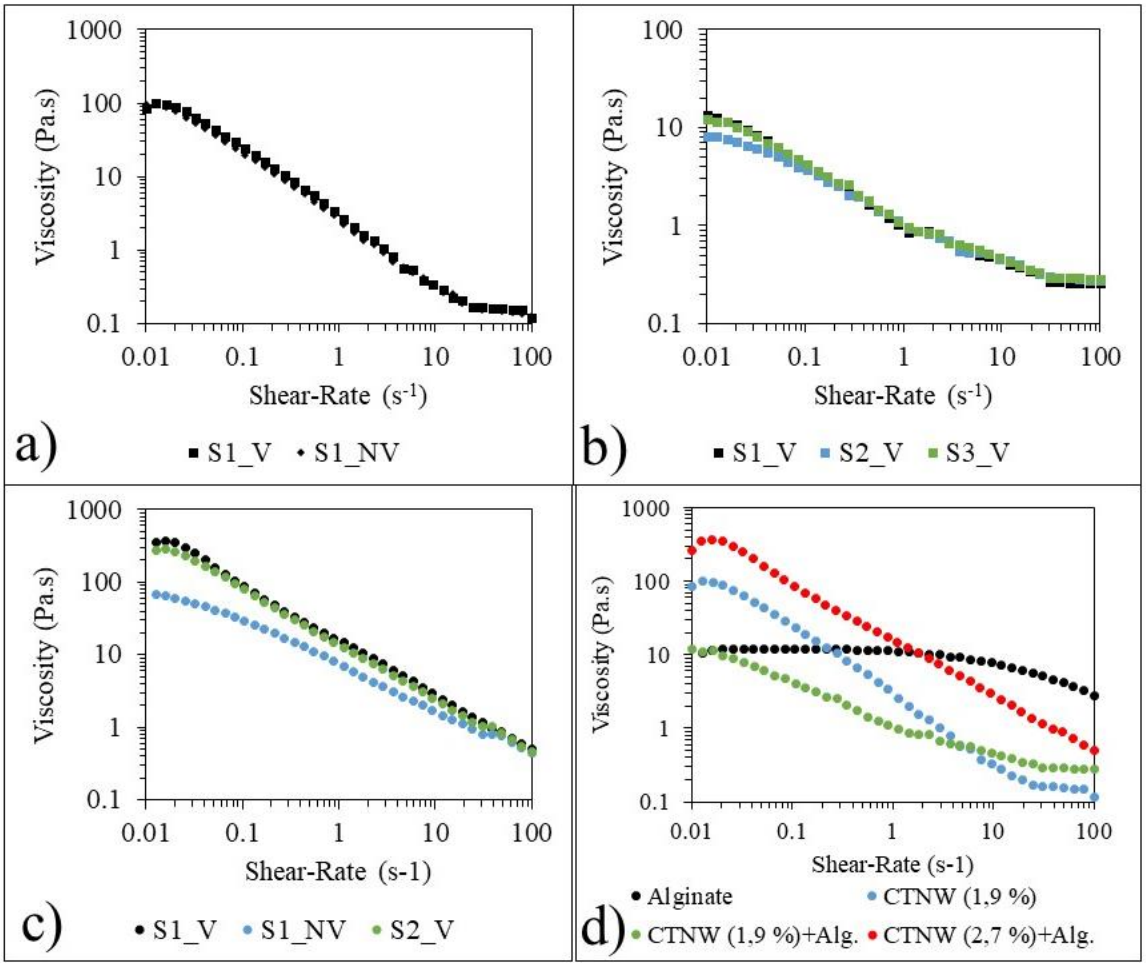

Figure 3.10 - Flow behaviour of: a) CTNW (1.9 % wt.) samples; b) CTNW (1.9 % wt.) with addition of alginate (4:1 volume ratio); c) CTNW (2.7 % wt.) with addition of alginate (4:1 volume ratio).d) Flow behaviour comparations between alginate and the samples of CTNW (1.9 % wt.), CTNW (1.9 % wt.):alginate (4:1 volume ratio) and CTNW (2.7 % wt.):alginate (4:1 volume ratio). S1, S2, S3 and S4 refers to the each sample used to the experiment, while V and NV indicates if the sample was virgin or non-virgin respectively.

Posteriorly, to study the gelation kinetics of our bioinks, we exposed them to different kinds of cross-linking solutions. In Figure 3.11 and Figure 3.12 are presented the gelation curves of our bioinks, and it is transversal to all experiments that both storage and loss modulus (G' and G" respectively) present higher values after the addition of the cross-linking solution.

In the gelation curve of CNC (1.9 % wt.):alginate (Figure 3.11) we notice that three minutes after the addition of the cross-linking solution, the G' overcomes the G". This cross point between G' and G" it is called 'gel point', it corresponds to a transition from a fluid-like (viscous) behavior where G">G to a solid-like (elastic) behavior where G'>G" [42]. This means that three minutes after the bioink meets the cross-linking solution, it forms a gel. Sixty seconds after the gel-point the storage and loss modulus stabilized.

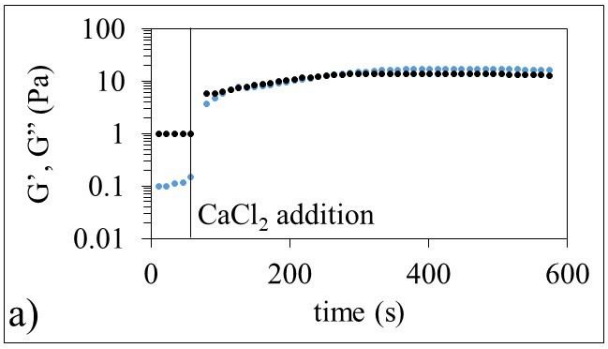

Figure 3.11 - Gellation curve of CNC(1.9 % wt.):alginate bioink before and after addition of PVA (10 % wt.) $CaCl_2$ 50 mM. Storage modulus (G') is represented by the blue curve while loss modulus (G") is represented by the black curve.

In the gelation curves of CTNW:alginate (Figure 3.12) the curve of G' overcomes the curve of G" even before the addition of cross-linking solution and this diverse behavior, when compared with the one observed for cellulose nanocrystals (Figure 3.11) might be due to the presence of carboxylate groups, from the N-acetylglucosamine functional group in the unit of chitin, that promotes physical interactions (van der Waals, hydrogen bonds, and electrostatic interactions). A similar behavior was described by Siqueira *et al.* [43] where the authors cross-linking the alginate with TEMPO-oxidized cellulose nanocrystals with Ca^{2+} ions to formulate hydrogels. Likewise, what is observed in the natural structure of chitin, these TEMPO-oxidized cellulose nanocrystals result from the functionalized of OH groups with many carboxylate groups which promote the ionic cross-linking between alginate and the CNCs. In Figure 3.12 from the observation of the curves of CTNW:alginate bioinks, it is possible to see that the G' is above the G" even before adding the $CaCl_2$, which might be related with the interactions between the carboxylate groups of chitin and alginate, which that behaves as a *quasi-gel*. A similar effect is observed by Liu *et al.* [44]for the effect of chitin nanocrystals on natural rubber. After adding the $CaCl_2$, the difference between G' and the G" curves increased through time due to the presence of more Ca^{2+} ions which promote the cross-linking of more carboxylate groups and therefore the formation of a gel.

It is also possible to see that the amplitude of G' and G" between the beginning and the end of the experience is ten times higher at the CTNW (1.9 % wt.):alginate bioink than the CTNW (2.7 % wt.):alginate bioink. Additionally, the stabilization of G' and G" curves is faster using the PVA (10 % wt.) $CaCl_2$ 50 mM cross-linking solution than the $CaCl_2$ 100 mM aqueous cross-linking solution.

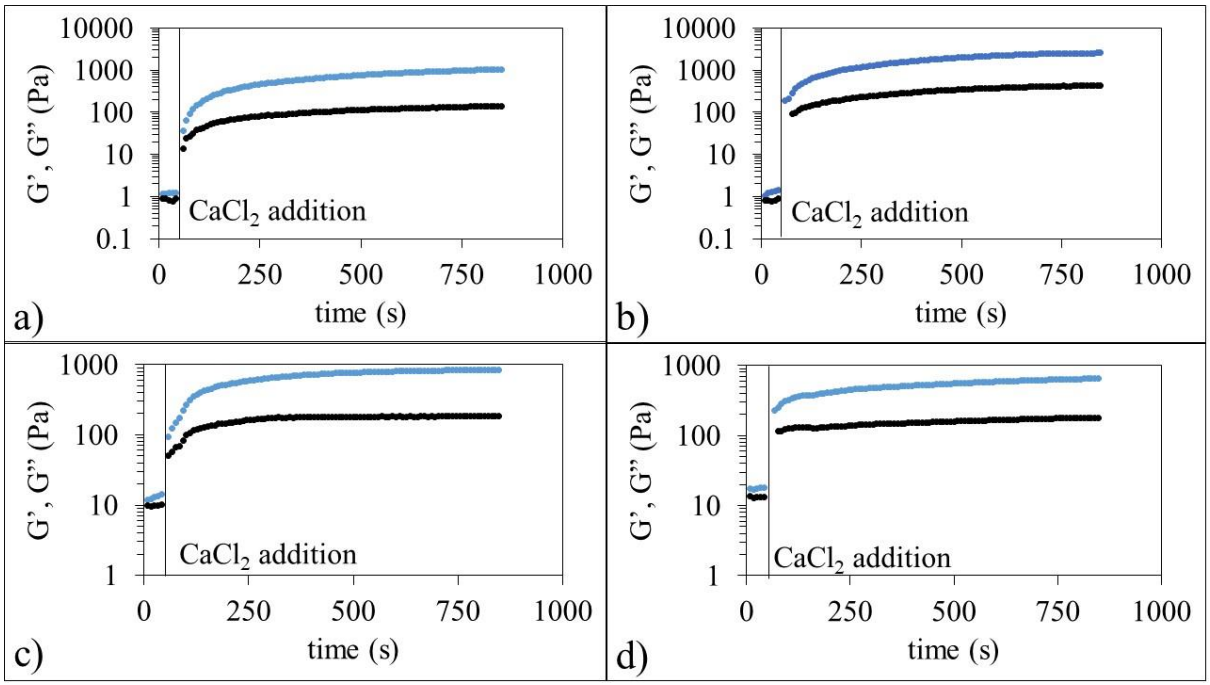

Figure 3.12 – Gellation curves of different CTNW:alginate bioinks before and after addition of different cross-linking solutions: a) CTNW (1.9 % wt.):alginate with addition of $CaCl_2$ 100 mM; b) CTNW (1.9 % wt.):alginate with addition of PVA (10 % wt.) $CaCl_2$ 50 mM; c) CTNW (2.7 % wt.):alginate with addition of $CaCl_2$ 100 mM; d) CTNW (1.9 % wt.):alginate with addition of PVA (10 % wt.) $CaCl_2$ 50 mM. Storage modulus (G') is represented by the blue curves while loss modulus (G") is represented by the black curves.

3.2 "Hand-draw 3D printing" of CNC and CTNW bionks

We resort to a "hand-draw 3D printing" technique for the purpose of evaluate the printability of the produced bionks. The experiments were firstly done with the CNC:alginate bioink in order to determine the conditions that allowed the impression and try to mimic what was obtained from Muller *et al.* [11] . Posteriorly, new tests were done with CTNW:alginate bioink, the object of study of this dissertation, to verify and if necessary, readjust the experimental conditions. Until the ideal conditions for "hand-draw 3D printing" were reached, several tests were performed. All the tests were performed within a Petri Dish with the cross-linking solution operating a syringe with a needle.

In the first approach a coverslip was placed in a Petri Dish and submersed with a PVA (5 % wt.) $CaCl_2$ (100 mM) cross-linking solution. Following by the deposition of CNC:alginate bioink on top of the coverslip. Due to the high concentration of $CaCl_2$ in the medium, the bioink's cross-linking was immediately observed leading to the bioink's detachment from the surface of the glass. The fast cross-linking reaction didn't permit the adhesion of the bioink to the coverslip and since the ink started to float this test is invalid.

We presumed that, for the same prior conditions, by first printing on the coverslip and then submerging it in the cross-linking solution it would promote adhesion of the ink to the glass substrate. However, this procedure also showed up to ineffective since did not allow the creation of 3D structures possible due to the high hydrophilicity of the glass.

For the third and fourth tests, we decided to increase the PVA concentration in the cross-linking solution to 10 % wt. and maintain the concentration of $CaCl_2$ with the view to increase the viscosity of the cross-linking solution and prevent the bioink from floating. On the third test the coverslip was submerged, and again, due to the high concentration of $CaCl_2$, the bioink immediately cross-linked and didn't adhere to the coverslip. Whereas on the fourth test, the printing was firstly done over the coverslip and then submerging it in the cross-linking solution. As observed in the previous tests, it was not possible to create 3D structures. For the following experiments, we decided to print with the substrate previously submerged.

At this point, we considered that reducing the concentration of $CaCl_2$ in the cross-linking solution from 100 mM to 50 mM would allow the adhesion of the bioink to the substrate. Therefore, for the sixth experiment, we used a cross-linking solution of $CaCl_2$ of 50 mM in ultrapure water. Although at the printing moment the bioink adhered to the coverslip, after 15 minutes it released from the substrate and started to float.

For the seventh test, a PVA 10 % wt. $CaCl_2$ 50 mM cross-linking solution was used in order to avoid the bioink from floating, but as it occurred in the previous test, after fifteen minutes the bioink started floating.

The eighth test ran at the same conditions as the seventh but with lower volume of cross-linking solution to promote the adhesion of the bioink to the coverslip. Twenty minutes after the printing, the coverslip was removed from the inside of the Petri Dish and therefore from the cross-linking solution, and we verified that although the bioink didn't float, it didn't adhere to the substrate. Additionally, due to low volume of cross-linking solution, there were regions of the bioink that didn't cross-linked. This was confirmed resorting a spatula.

The ninth test was performed using a cross-linking solution of PVA 10 % wt. and $CaCl_2$ 25 mM at low volume, in order to promote adhesion to the substrate. After thirty minutes, we confirmed that the cross-linking was successful, although the bioink didn't adhere to the coverslip.

At this point, we understood that to resolve the adhesion problem of previous test, we must substitute the coverslip substrate for other substrates.

Finally, for the tenth and eleventh test, we decided to use aluminum foil as a substrate. For both tests, a PVA 10 % wt. $CaCl_2$ 25 mM cross/linking solution was used. At these conditions, was possible to "hand-draw" a structure over the substrate which was removed from the cross-linking solution after

twenty minutes. After the washing and drying processes, we obtained the first successfully printed structures.

The twelfth experiment was performed over a universal plain paper, at the same cross-linking conditions as the eleventh test. We considered these conditions as the triumphant ones and we used them through the following tests with CNC:alginate bioink. The Figure 3.13 shows three successful "hand-drawn 3D printed" structures and the Figure 6.3 presents photos of all tests previously described.

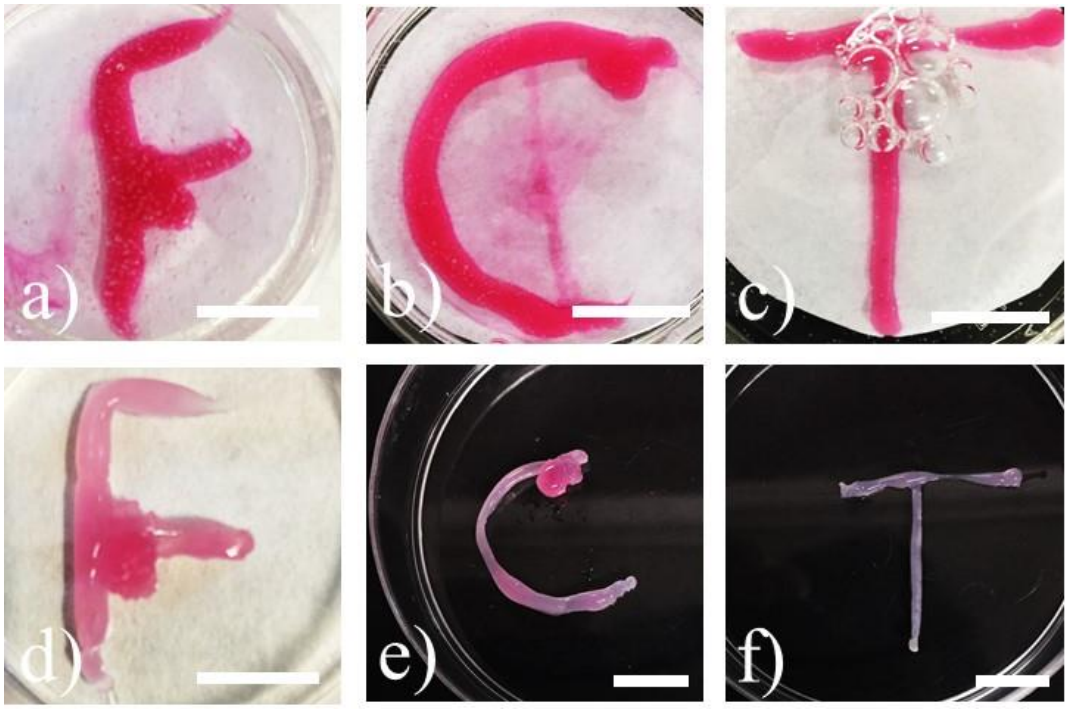

Figure 3.13 – "Hand-drawn 3D print" successful structures with CNC:alginate bioink. a), b) and c) show the bioink at the moment of printing. d), e) and f) show the structures twenty minutes after cross-linking, washing and drying processes. The pink coloration is due to the use of a dye in the bioink Scale bars: 1 cm.

Considering the conditions of the previous well succeeded tests, new "hand-draw 3D printing" experiments were made, this time with CTNW (1.9 % wt.):alginate bioink.

The first test was performed at a CTNW (1.9 % wt.):alginate ratio of 4.2:1, over a plain paper submersed in a PVA 10 % wt. $CaCl_2$ 25 mM cross-linking solution. After twenty minutes, we confirmed with a spatula, that the structure wasn't fully cross-linked, which was once more confirmed after sixty minutes. Since we had previously determined with the CNC: alginate bioink, the conditions for well succeeded printing such as type of substrate and cross-linking solution's concentration, we supposed that lowering the bioink ratio, we would accomplish the robustness of the structure within a twenty-minute gap. In the Table 3.2 it is resumed the results of qualitative robustness of the structures.

We concluded two facts: primarily that the longer the bioink was cross-linking, the better robustness it would present; in second place, that the lower the ratio between CTNW and alginate, the better robustness it would present as well the fastest it would present.

Table 3.2 – Resume of the results of qualitative structures robustness. The X its for bad robustness; the V its for good robustness; and the VV its for very good robustness.

CTNW:alginate ratio	**4:1**		**3.5:1**		**3:1**		**2.5:1**	
Time (minutes)	20	60	20	60	20	60	20	60
PVA 10 % wt. $CaCl_2$ 25 mM	X	X	V	V	V	VV	V	VV
PVA 10 % wt. $CaCl_2$ 50 mM	V	V	V	V	V	VV	V	VV

In the Figure 3.14 are presented well succeeded printings with CTNW (1.9 % wt.):alginate bioink, as well as in the Figure 6.4.

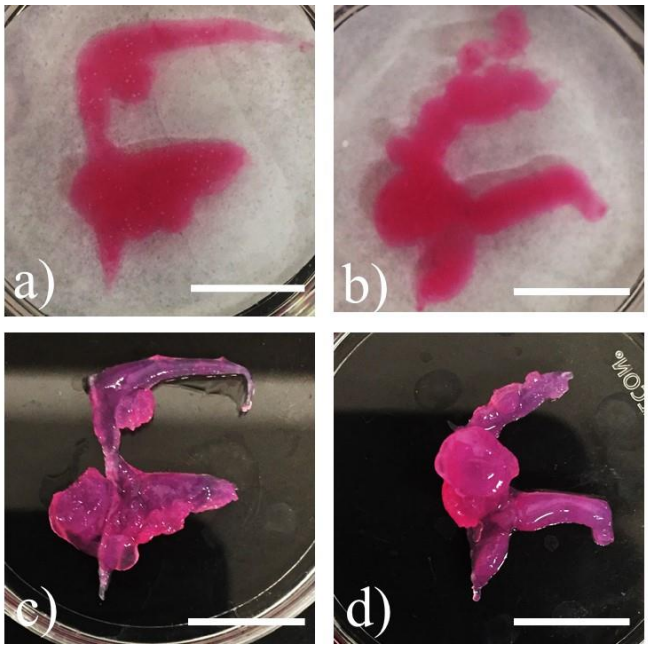

Figure 3.14 - "Hand-drawn 3D printed" structures with CTNW:alginate bioink at a 3:1 ratio. a) and b) show the bioink at the moment of printing while c) and d) show the structures sixty minutes after cross-linking, washing and drying processes. The pink coloration is due to the use of dye in the bioink. Scale bars: 1 cm.

In order to evaluate the capacity of the bioinks to absorb and retain water after the cross-linking mechanisms, we analyze the weight swelling ratio of samples of hydrogels produced from the bioinks. Figure 3.15 represents the mass swelling ratio of CNC (1.9 % wt.):alginate hydrogels obtained three different cross-linking solutions. The determination of the weight swelling (S_w) ratio, corresponding to the hydrogels' water uptake, was determined according to the following equation:

$$S_w\ (\%\ \mathrm{wt.}) = \left(\frac{w_t - w_0}{w_0}\right) 100$$

w_t represent the weight of the swollen hydrogel at a specific time *t* and w_0 is the initial weight of the sample before swelling.

From Figure 3.15 all samples reached a maximum water uptake after being immersed for 3 hours in ultrapure water. At this time the stabilization of the mass swelling ratio occurs, and the hydrogels showed a maximum of swelling of 54 % wt., 154 % wt. and 163 % wt. for $CaCl_2$ 100 mM, PVA (10 % wt.) $CaCl_2$ 50 mM and PVA (10 % wt.) $CaCl_2$ 25 mM cross-linking aqueous solutions, respectively. The values obtained for the cross-linking solutions derived only from $CaCl_2$ are in good agreement with the values obtained by Asadi *et at.* [45] for air-dried beads of alginate:CNC. Higher values of water uptake (200% wt.) were obtained by Jayaramudu *et al.* [46] for hydrogels of CNC/PVA (obtained from freeze/thaw procedure). It is important to note that a straight comparison with these studies is difficult since the hydrogel precursor solution and cross-linking solutions does not have the same composition of each material.

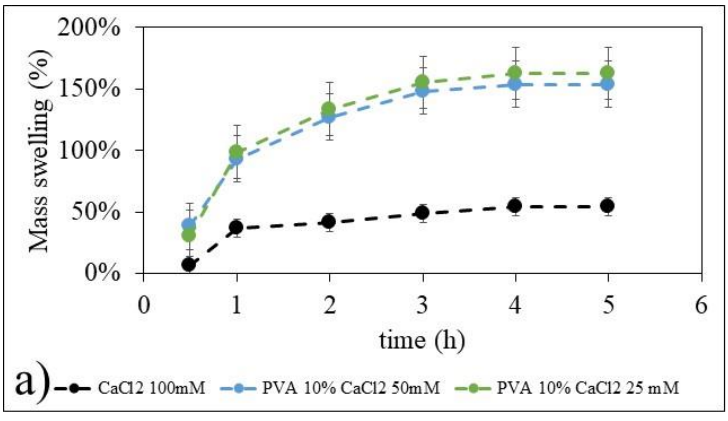

Figure 3.15 – Swelling behaviour of CNC (1.9 % wt.):alginate hydrogel.

Figure 3.16 represents the weight swelling ratio of CTNW:alginate hydrogels, obtained from three different cross-linking solutions. In the first study the hydrogels were obtained with a suspension of

CTNW (1.9 % wt.):alginate and the second with CTNW (2.7 % wt.):alginate (Figure 3.16 a) and b)). It can be see that the hydrogels reach its equilibrium swelling state approximately after 3 hours of being immersed in ultrapure water, as the weight swelling ratio stabilizes. The maximum weight swelling ratio of CTNW (1.9 % wt.):alginate hydrogels is 12 % wt., 45 % wt. and 82 % wt. for $CaCl_2$ 100 mM aqueous, PVA (10 % wt.) $CaCl_2$ 50 mM and PVA (10 % wt.) $CaCl_2$ 25 mM cross-linking solutions respectively. While the maximum mass swelling ratio of CTNW (2.7 % wt.):alginate bioink were at 17 % wt., 71 % wt. and 61 % wt. for $CaCl_2$ 100 mM aqueous, PVA (10 % wt.) $CaCl_2$ 50 mM and PVA (10 % wt.) $CaCl_2$ 25 mM cross-linking solutions respectively.

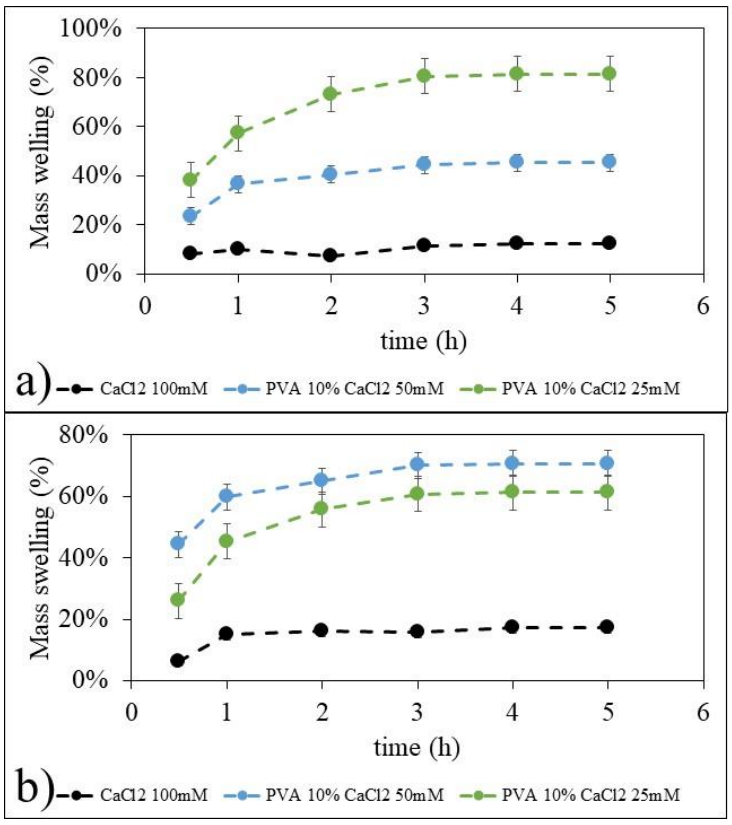

Figure 3.16 - Swelling behaviour of a) CTNW (1.9 % wt.):alginate and b) CTNW (2.7 % wt.):alginate hydrogels.

From the swelling behaviour presented above one can see that the changes in cross-linking solutions is a good strategy for controlling the water uptake and therefore modulating the swelling behavior of the produced hydrogels.

3.3 3D printing

The 3D printing process, as well as the "hand-draw 3D printing", underwent several changes as we performed the tests and the experiments were firstly made with CNC, used as a model, and then replicate with CTNW. Since it wasn't possible to print inside any container do to the 3D printer calibration, we started the experiments with two different approaches: with a plain paper previously embedded in the cross-linking solution as a substrate and after with a glass substrate. In the first approach, it was not possible to print because the bioink wouldn't adhere to the paper substrate and so, the printer couldn't print the designed structure. For the second approach we decided to print over a glass substrate and at the end of printing each layer, we sprayed the structure with the cross-linking solution in order to attribute some robustness to this layer in order to be able to support the following layers.

In the Figure 3.17 are presented the obtained 3D printed structures of CNC. In the first row of the Figure 3.17 there is liquid present over the substrate which corresponds to the cross-linking solution sprayed. The "F", "C" and "T" structures, in both kinds of bioink, have slightly rounded corners due to the lack of support ability of the lower layers. Although it was possible to print a 3D structure (Figure 3.13) with the optimized experimental condition established on the "hand-drawn printing" system, when these conditions were transported to the 3D printing process the obtained structures were highly irregular. In order to obtain a true 3D structure of this composite material further studies had to be done, mainly related with the cross-linking procedure while the printing process was done, but also an increase in the viscosity of the suspensions should be obtained. This last suggestion arises from the fact that while printing it was noticeable that the CNC: alginate mixtures did not present a laminar flow and this flow turbulence might also be responsible for the results see in this figure. Nevertheless, CNC:alginate is not the focus of our study and from the CNC:alginate characteristics presented below they cannot be compared with the CNF: alginate bioink presented by Muller *et al.*[11].

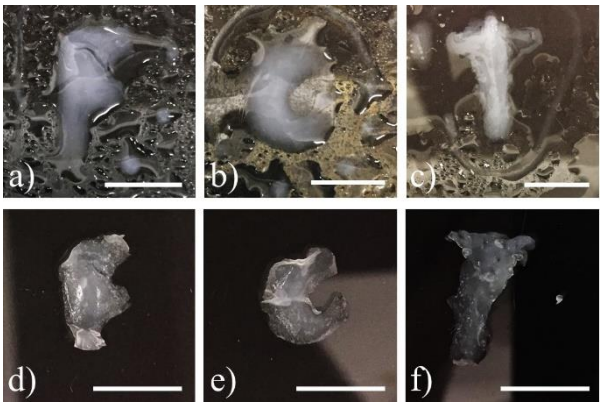

Figure 3.17 – 3D printed structures of CNC:alginate bioink. In the first row the pictures were taken at the time the printing was finished; in the second where are the structures obtained after washing and drying procedures. Scale bars: 1 cm.

In the Figure 3.18 are presented the obtained 3D printed structures of CTNW (1.9 % wt.). If we compare the structures obtained with the ones of CNC:alginate hydrogel a better result is obtained, however this was not what is expected. Since it was not possible to 3D print directly inside the cross-linking solution we try to optimize the printing flow, since with this CTNW concentration it was turbulent.

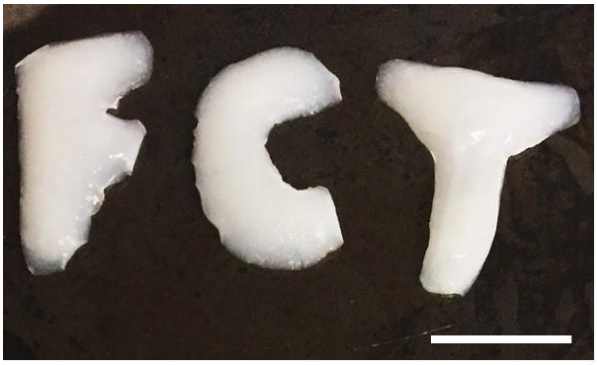

Figure 3.18 – 3D printed structures of CTNW (1.9 % wt.):alginate bioink. Scale bar: 1 cm.

The flow of a fluid in a pipe (as our printing needle) can be related with the Reynolds number. The importance of the viscosity of the fluid is evident in the following equation of Reynolds number (1)

$$\boldsymbol{R = \frac{\rho v D}{\mu}} \qquad (1)$$

where, R is the Reynolds number (unitless), ρ is the fluid density (kg/m^3), v is the velocity of the fluid (m/s), D is the diameter of the needle (m), μ is the viscosity of the fluid (Pa.s). From this equation one

can relate that an increase in the viscosity of the fluid will originate a lower Reynold number. If the Reynolds number is less than 2,300, the flow of the fluid is laminar and if it is above 4,000, the flow is turbulent. Since the objective was to have a laminar flow when extruding the bioink to avoid the drop formation at the tip of the needle, the CTNW (2.7 % wt.):alginate bioink, which was the bioink with higher viscosity for low shear rate, was theoretically the best option for 3D printing.

In Figure 3.19 and Figure 3.20 is presented a successful 3D printed structure using a CTNW (2.7 % wt.):alginate bioink, which proves that chitin nanowhiskers are a excellent choice to use viscosity modifiers even at low concentrations of CTNW and low CTNW:alginate volume ratios.

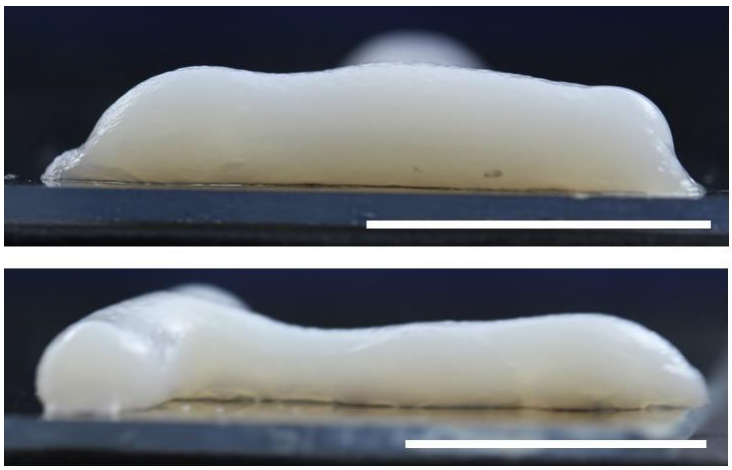

Figure 3.19 - 3D printed structure of CTNW (2.7 % wt.):alginate bioink (side views). Scale bars: 1 cm.

Figure 3.20 - 3D printed structure of CTNW (2.7 % wt.):alginate bioink (top view) Scale bar: 1 cm.

4 Conclusion and future perspectives

This dissertation's main goal was the production and characterization of hydrogels derived from alginate and nanochitin particles and evaluate its 3D printability as bioinks. By manipulating different variables like the substrate, the concentration of nanoparticles and cross-linking solutions, along with the variety of characterization methods employed, allows us to assert that a significant amount of progress was made on the subject.

A parallel study was performed with cellulose nanocrystals as a model, in order to produced 3D printed structures as the ones obtained in the literature [11] for nanofibrillated cellulose and accessed methodology to be used in the nanochitin suspension systems. For this, cellulose nanocrystals were successfully obtained from the acid hydrolysis of microcrystalline cellulose. Starting from a particle size of ~50 μm it was possible to obtain rods with average 135 ± 48 nm of length and 4 ± 1 nm of diameter. These equates to an approximate aspect ratio (*L/d*) of 38:1. The diffraction patterns of CMC and CNC showed the presence of a cellulose type Iβ polymorph structure which confirms the stability of the structure across both samples. The CNC sample presents a higher crystalline index (IC = 81 % wt.) when compared to the CMC crystalline index (IC = 77 % wt.). Through the mass swelling ratio curves, it was possible to confirm that the CNC (1.9 % wt.):alginate hydrogel features such as capacity to absorb and retain water inside its structure. The samples reached a maximum and stabilized the mass swelling ratio at 54 % wt., 154 % wt. and 163 % wt. for $CaCl_2$ 100 mM aqueous, PVA (10 % wt.) $CaCl_2$ 50 mM and PVA (10 % wt.) $CaCl_2$ 50 mM cross-linking solutions respectively. Rheological characterization indicates that at 0.01 s^{-1} shear-rate, the viscosity of the CNC aqueous solutions and CNC:alginate bioink (20 Pa.s and 9 Pa.s respectively) are slightly higher than alginate's viscosity (2 Pa.s). Gelation curves confirmed the successful cross-linking of the CNC:alginate bioink just after three minutes.

Chitin nanowhiskers were also successfully obtained from acid hydrolysis of chitin derived from shrimp shells. On average, the dimensions length, diameter and aspect ratio (*L/d*) were calculated to be 344 ± 127 nm, 6 ± 1 nm and 54:1, respectively. The CTNW's diffraction patterns show the presence of pure α-chitin, indicating that the crystal integrity was maintained after the hydrolysis process, however the CTNW presents a higher crystalline index (IC = 94 %) than chitin (IC = 83 %). Mass swelling ratio curves of CTNW (1.9 % wt.):alginate and CTNW (2.7 % wt.):alginate bioinks allow us to consider both CTNW:alginate bioinks as hydrogels due to its capacity to absorb and retain water inside its structures. The maximum mass swelling ratio of CTNW (1.9 % wt.):alginate bioink were at 12 % wt., 45 % wt. and 82 % wt. for $CaCl_2$ 100 mM aqueous, PVA (10 % wt.) $CaCl_2$ 50 mM and PVA (10 % wt.) $CaCl_2$ 50 mM cross-linking solutions respectively, while the maximum mass swelling ratio of CTNW (2.7 % wt.):alginate bioink were at 17 % wt., 71 % wt. and 61 % wt. for $CaCl_2$ 100 mM

aqueous, PVA (10 % wt.) $CaCl_2$ 50 mM and PVA (10 % wt.) $CaCl_2$ 50 mM cross-linking solutions respectively. Flow behavior characterization indicates that at 0.01 s^{-1} shear-rate, the viscosity of the CTNW (1.9 % wt.) aqueous solutions, CTNW (1.9 % wt.):alginate and CTNW (2.7 % wt.):alginate bioinks (100 Pa.s, 10 Pa.s and 300 Pa.s respectively) are two order of magnitude higher than alginate's viscosity. Gelation curves confirmed the successful cross-linking of the CTNW:alginate bioinks. The bioink with high concentration of CTNW was used to successfully print a 3D structure. And to the best of our knowledge it's the first time that nanochitin particles are used in alginate solution to give rise to 3D printed structures.

Although successful 3D structure was obtained with the CTNW:alginate bioinks, further improvements in the printed method should be performed.

1) We can further develop a support system, large enough to be outside printer's calibration point, which will allow the production of the structure inside the cross-linking solution, and therefore, ensure the homogeneous cross-linking of the structure.

2) Determined the optimal 3D printing conditions by studying the effect of several parameters that affect the laminar flow as the needle diameter or increase of bioink viscosity.

3) Determined the optimal composition of the cross-linking solution to be used with the 3D printer.

5 References

1. Mironov, V., et al., *Organ printing: computer-aided jet-based 3D tissue engineering.* Trends in Biotechnology, 2003. **21**(4): p. 157-161.
2. Melek, L.N., *Tissue engineering in oral and maxillofacial reconstruction.* Tanta Dental Journal, 2015. **12**(3): p. 211-223.
3. Williams, D., et al., *A Perspective on the Physical, Mechanical and Biological Specifications of Bioinks and the Development of Functional Tissues in 3D Bioprinting*. Bioprinting, 2018, **9**.: p. 19-36.
4. Aljohani, W., et al., *Bioprinting and its applications in tissue engineering and regenerative medicine.* International Journal of Biological Macromolecules, 2018. **107**(PartA): p. 261-275.
5. Ozbolat, I.T., W. Peng, and V. Ozbolat, *Application areas of 3D bioprinting.* Drug Discovery Today, 2016. **21**(8): p. 1257-1271.
6. Mandrycky, C., et al., *3D bioprinting for engineering complex tissues.* Biotechnology Advances, 2016. **34**(4): p. 422-434.
7. Gungor-Ozkerim, P.S., et al., *Bioinks for 3D bioprinting: An overview.* Biomaterials Science, 2018. **6**(5): p. 915-946.
8. Parak, A., et al., *Functionalizing bioinks for 3D bioprinting applications.* Drug Discovery Today, 2018. **24**(1): p. 1-8.
9. Ahmed, E.M., *Hydrogel: Preparation, characterization, and applications: A review.* Journal of Advanced Research, 2015. **6**(2): p. 105-121.
10. Merceron, T.K. and S.V. Murphy, *Chapter 14 - Hydrogels for 3D Bioprinting Applications*, in *Essentials of 3D Biofabrication and Translation*, A. Atala and J.J. Yoo, Editors. 2015, Academic Press: Boston. p. 249-270.
11. Müller, M., et al., *Alginate Sulfate–Nanocellulose Bioinks for Cartilage Bioprinting Applications.* Annals of Biomedical Engineering, 2017. **45**(1): p. 210-223.
12. Li, G., et al., *Structure and properties of chitin/alginate blend membranes from NaOH/urea aqueous solution.* International Journal of Biological Macromolecules, 2012. **51**(5): p. 1121-1126.
13. *Cellulose Nanocrystals: Properties, Production and Applications by Wadood Y. Hamad.* MRS Bulletin, 2018. **43**(6): p. 461-461.
14. Wada, M., et al., *Cellulose IIII Crystal Structure and Hydrogen Bonding by Synchrotron X-ray and Neutron Fiber Diffraction.* Macromolecules, 2004. **37**(23): p. 8548-8555.
15. Phanthong, P., et al., *Nanocellulose: Extraction and application.* Carbon Resources Conversion, 2018. **1**(1): p. 32-43.
16. Araki, J., et al., *Influence of surface charge on viscosity behavior of cellulose microcrystal suspension.* Journal of Wood Science, 1999. **45**(3): p. 258-261.

17. Huq, T., et al., *Nanocrystalline cellulose (NCC) reinforced alginate based biodegradable nanocomposite film.* Carbohydrate Polymers, 2012. **90**(4): p. 1757-1763.

18. João, C.F.C., et al., *Natural Nanofibres for Composite Applications*, in *Fibrous and Textile Materials for Composite Applications*, S. Rana and R. Fangueiro, Editors. 2016, Springer Singapore: Singapore. p. 261-299.

19. João, C.F.C., et al., *Bio-inspired production of chitosan/chitin films from liquid crystalline suspensions.* Carbohydrate Polymers, 2017. **155**(2): p. 372-381.

20. Rinaudo, M., *Chitin and chitosan: Properties and applications.* Progress in Polymer Science, 2006. **31**(7): p. 603-632.

21. João, C. F. C., et al., *Inverted Colloidal Crystal Scaffolds: New Substitutes for Bone Tissue Engineering.* PhD Thesis, FCT-UNL, 2016.

22. Nguyen, D., et al., *Cartilage Tissue Engineering by the 3D Bioprinting of iPS Cells in a Nanocellulose/Alginate Bioink.* Scientific Reports, 2017. **7**(1): p. 1-10.

23. Liu, J., et al., *Current advances and future perspectives of 3D printing natural-derived biopolymers.* Carbohydrate Polymers, 2019. **207**(1): p. 297-316.

24. Markstedt, K., et al., *Biomimetic Inks Based on Cellulose Nanofibrils and Cross-Linkable Xylans for 3D Printing.* ACS Applied Materials and Interfaces, 2017. **9**(46): p. 40878-40886.

25. Martínez Ávila, H., et al., *3D bioprinting of human chondrocyte-laden nanocellulose hydrogels for patient-specific auricular cartilage regeneration.* Bioprinting, 2016. **1-2**: p. 22-35.

26. Almeida, C.R., et al., *Impact of 3-D printed PLA- and chitosan-based scaffolds on human monocyte/macrophage responses: Unraveling the effect of 3-D structures on inflammation.* Acta Biomaterialia, 2014. **10**(2): p. 613-622.

27. Demirtaş, T., G. Irmak, and M. Gumusderelioglu, *Bioprintable form of chitosan hydrogel for bone tissue engineering*. Biofabrication, 2017, **9**(3): p. 035003.

28. Elviri, L., et al., *Highly defined 3D printed chitosan scaffolds featuring improved cell growth*. Biomed Mater, 2017, **12**(4): p. 045009.

29. Fernandes, S.N., et al., *Mind the Microgap in Iridescent Cellulose Nanocrystal Films.* Advanced Materials, 2017. **29**(2): 1603560.

30. Gaspar, D., et al., *Nanocrystalline cellulose applied simultaneously as the gate dielectric and the substrate in flexible field effect transistors.* Nanotechnology, 2014. **25**(9): 094008.

31. Asri, S. E. A. M., et al., *Isolation and Characterization of Chitin Nanowhiskers from Fermented Tiger Prawn Waste*. Chemical Engineering Transactions, 2017. **56**: p. 139-144.

32. Vasconcelos, N.F., et al., *Bacterial cellulose nanocrystals produced under different hydrolysis conditions: Properties and morphological features.* Carbohydrate Polymers, 2017. **155**: p. 425-431.

33. C. Segal, L., et al., *An Empirical Method for Estimating the Degree of Crystallinity of Native Cellulose Using the X-Ray Diffractometer*. Textile Research Journal, Vol. 29. 1959: p. 786-794.

34. Clark, G.L. and A.F. Smith, *X-ray Diffraction Studies of Chitin, Chitosan, and Derivatives.* The Journal of Physical Chemistry, 1935. **40**(7): p. 863-879.

35. Honorato-Rios, C., et al., *Fractionation of cellulose nanocrystals: enhancing liquid crystal ordering without promoting gelation*. NPG Asia Materials, 2018, **10**: p. 455-465.

36. Atalla, R. H. and Isogai, A., *Recent Developments in Spectroscopic and Chemical Characterization of Cellulose*. Polysaccharides: structural diversity and functional versatility. New York: Marcel Dekker, 2005: p. 123-157.

37. Martins, M., et al., *Extraction and characterization of cellulose whiskers from commercial cotton fibers*. Journal of Materials Science, 2011, **46**(24): p. 7858-7864.

38. Moussout, H., et al., *Kinetics and mechanism of the thermal degradation of biopolymers chitin and chitosan using thermogravimetric analysis.* Polymer Degradation and Stability, 2016. **130**: p. 1-9.

39. Stawski, D., et al., *Thermogravimetric analysis of chitin of different origin*. Journal of Thermal Analysis and Calorimetry, 2008, **93**(2): p. 489-494.

40. Bercea, M. and P. Navard, *Shear Dynamics of Aqueous Suspensions of Cellulose Whiskers.* Macromolecules, 2000. **33**(16): p. 6011-6016.

41. Li, W., et al., *The liquid crystalline order, rheology and their correlation in chitin whiskers suspensions*. Carbohydrate Polymers, 2019, **209**(1): p. 92-100.

42. Macosko, C.W., *Rheology: principles, measurements, and applications*. Advances in interfacial engineering series. New York, Wiley-VCH, 1994: p. 1-535

43. Siqueira, P., et al., *Three-Dimensional Stable Alginate-Nanocellulose Gels for Biomedical Applications: Towards Tunable Mechanical Properties and Cell Growing*. Nanomaterials, 2019, **9**(1): p. 78.

44. Liu, Y., et al., *Liquid Crystalline Behaviors of Chitin Nanocrystals and Their Reinforcing Effect on Natural Rubber*. ACS Sustainable Chemistry & Engineering, 2017, **6**(1): p. 325-336.

45. Asadi, S., S. Eris, and S. Azizian, *Alginate-Based Hydrogel Beads as a Biocompatible and Efficient Adsorbent for Dye Removal from Aqueous Solutions.* ACS omega, 2018. **3**(11): p. 15140-15148.

46. Jayaramudu, T., et al., *Electroactive Hydrogels Made with Polyvinyl Alcohol/Cellulose Nanocrystals*. Materials, 2018, **11**(9): 1615.

47. Faria, J., et al., *Towards the development of multifunctional hybrid fibrillary gels: production and optimization by colloidal electrospinning.* RSC Adv., 2017. **7**(77): p. 48972-48979.

6 Supporting Information

6.1 Methods to chemical, structural and dimensional characterization

Chemical characterization via Fourier Transform Infrared spectroscopy (FTIR) was conducted on samples of dried microcrystalline and nanocrystalline cellulose, and on samples of chitin and nanochitin. FTIR data were recorded using an Attenuated Total Reflectance (ATR) sampling accessory (Smart iTR) equipped with a single bounce diamond crystal on a Thermo Nicolet 6700 spectrometer. The spectra were acquired at a room temperature of 25 ºC, with a 45 ° incident angle in the range of 4,000 to 525 cm^{-1} and with a 4 cm^{-1} resolution.

The samples of microcrystalline and nanocrystalline cellulose, as well as the samples of chitin and chitin nanowhiskers were structurally and dimensionally characterized using X-Ray Diffraction (XRD), Thermogravimetric analysis and Differential Scanning Calorimetry (TG/DSC), and Atomic Force Microscopy (AFM).

XRD curves were obtained using a PANalytical X'pert PRO model diffractometer, with Bragg-Brentano (θ/2θ coupled) geometry with graphite monochromated Cu KR (1.54 Å) radiation. Data was collected at a scanning step of 2θ=0.0334 º, from 10 º to 40 º.

Thermogravimetric analysis measurements were performed using a Netzsch 449 F3 Jupiter® simultaneous thermal analyzer where each sample was heated from 20 to 900 ºC, at a heating rate of 10 ºC/min.

Atomic Force Microscopy (AFM) data was acquired using an Asylum Research MFP-3D standalone system in tapping mode, with commercially available silicon AFM probes (scanning frequency of 300 kHz, k = 26 N/m). The analyzed particles were prepared by casting 1 μL droplets of an ultra-diluted suspension in water (0.01 % w/w) on top of a fresh half-open mica substrate (Muscovite Mica, V-5 from Electronic Microscopy Sciences). Immediately before deposition, the suspension was sonicated for two consecutive cycles of 10 min over an ice bath using a Hielscher UP400S ultrasonic homogenizer(460W, 24 kHz, 0.85 of the cycle and 80 % amplitude).

The measurements of diameter (*d*), length (*L*) and aspect ratio (*L/d*) for our CNC and CTNW rods were made by carrying out single profile measurements with the software Gwyddion (version 2.50, http://gwyddion.net). To get a truly representative measure of *d*, we found that the commonly used method of measuring an AFM height profile perpendicular to each rod at some randomly chosen crossing point was insufficient, due to the considerable height variations along every individual rod. Instead, we measured the height profile along each rod *r* and the average value was used as its

diameter, d_r. For each sample, 160 rods were measured individually and by averaging $\underline{d_r}$ obtained for each of these we thus determined a final representative diameter value *d*.

6.2 Swelling behaviour and rheological characterization

Weght swelling ratio properties of CNC (1.9 % wt.):alginate, CTNW (1.9 % wt.):alginate and CTNW (2.7 % wt.):alginate bioinks after immersion of 5 samples in different cross-linking solutions for 30 minutes. After being washed with ultrapure water to stop the cross-linking mechanism, all the samples were dried in a temperature-controlled environment at 60 ºC for three days until there were no changes in the mass of the samples. The samples were then immersed in ultrapure water for 0.5, 1, 2, 3, 4 and 5 h. Between each immersion time the water was changed in order to minimize any possible single polymer chains resulting from the dissolution to reattach to the bioinks' samples [47].

Rheological characterization was made by rheological experiments on a Bohlin Gemini HRnano rotational rheometer. The measurements were performed using a plate-plate geometry (20 mm diameter and 1 mm gap size) at 25 ºC. To evaluate the flow behavior, shear-rate was increased from 0.01 to 100 s^{-1}. For the calcium gelation experiments, oscillatory measurements were performed at a frequency of 1 Hz and 0.05 % strain. The samples were equilibrated for 60 s before the addition of 100 mM $CaCl_2$ and subsequent measurement of gelation process for 10 min

6.3 Analysis of AFM data

Accurate measurements of diameter *d*, length *L* and aspect ratio *L/d* for our CNC rods and CTNW were obtained by carrying out single profile measurements with the software Gwyddin 2.52, based on a method presented by *Honorato-Rios, et al.* [35]. To get a truly representative measure of *d*, we found that the commonly used method of measuring an AFM height profile perpendicular to each rod at some randomly chosen crossing point was insufficient, due to the considerable height variations along every individual rod. Instead, we measured the height profile along each rod *r* (inset, Figure 6.1 and Figure 6.2) and the average value was used as its diameter, d_r. For CNC sample 159 rods were measured individually while for CTNW sample 109 rods were measured. By averaging d_r obtained for each rod we determined a final representative average diameter value $\bar{d}$ for each sample.

To obtain the length L_r of each rod r regardless of its orientation in the sample plane, we used the extension of the rod in the lab frame's *x* and *y* directions, Δx_r and Δy_r, which are directly available from the height profile data. We then applied the Pythagorean theorem to calculate the length as $L_r = \sqrt{\Delta x_r^2 + \Delta y_r^2}$, as indicated in Figure 6.1 and in Figure 6.2. An average length value $\bar{L}$, was again calculated as the average of all L_r values established for all the rods. Finally, for each rod *r* we

determined the aspect ratio as L_r/d_r, and the aspect ratio chosen to represent the sample was the average $\overline{L/d}$ of the aspect ratio of every rod.

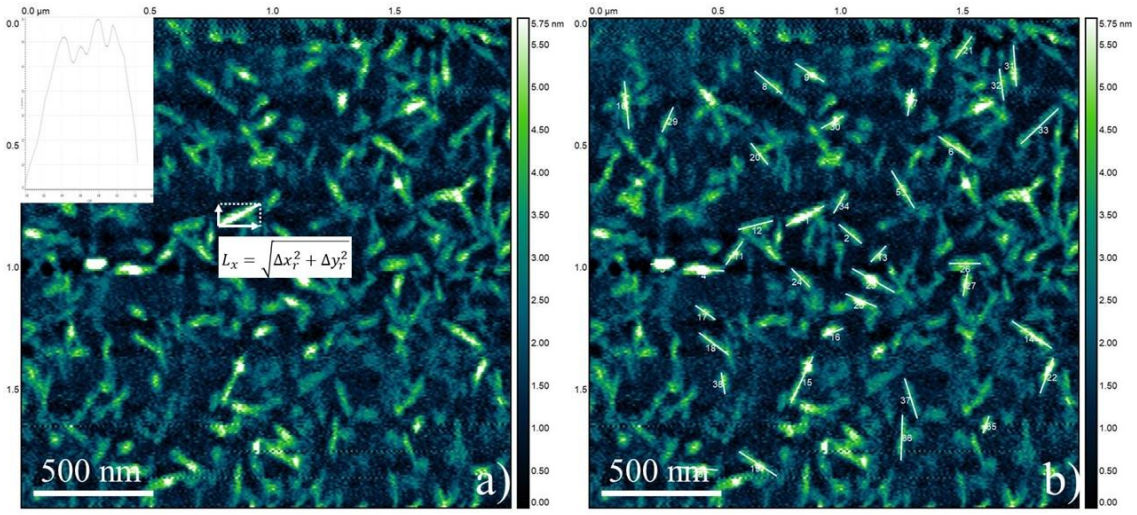

Figure 6.1 - AFM images of a random CNC sample as example of the determination of diameter d, length L and aspect ratio L/d of CNC rods. a) Original image with an example of the height profile along one rod (inset), showing how d changes along the length of a typical rod. b) 38 rods measured by using the profile tool (an Excel file with all profile data is included as separate Supporting Information file).

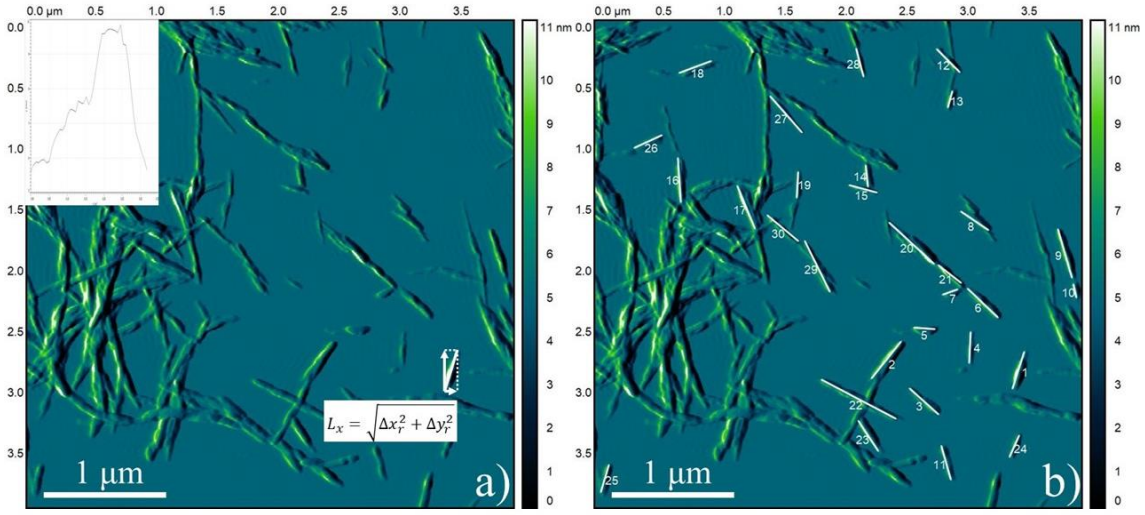

Figure 6.2 - AFM images of a random CTNW sample as example of the determination of diameter d, length L and aspect ratio L/d of CTNW. a) Original image with an example of the height profile along one rod (inset), showing how d changes along the length of a typical rod. b) 30 rods measured by using the profile tool (an Excel file with all profile data is included as separate Supporting Information file).

Table 6.1 – Average aspect ratio of CNC and CTNW samples.

		CNC	CTNW
Length (L, average)	nm	135.1	343.6
STD	nm	47.6	127
Diameter (d, average)	nm	3.6	6.4
STD	nm	0.7	1.3
Aspect Ratio (L/d, average)		61.5	79

Table 6.2 - AFM measurements of length (L_r) and diameter (d_r) of individual CNC rods.

L_r	d_r	L_r	d_r	L_r	d_r	L_r	d_r	L_r	d_r
177.7	5.0	212.4	3.6	152.3	2.6	115.3	3.2	109.4	3.6
122.7	3.9	91.0	3.8	206.6	2.4	130.5	3.7	73.9	3.7
100.1	5.2	73.9	4.6	171.7	2.4	167.0	3.2	76.8	3.4
166.9	4.9	188.1	3.4	137.3	2.7	159.1	3.8	97.1	2.9
181.0	3.8	171.7	3.3	42.1	2.8	132.9	2.7	168.2	3.5
154.8	4.7	89.3	3.6	109.9	2.4	84.3	3.4	95.0	3.7
113.7	4.2	312.3	2.3	85.0	2.5	112.5	2.6	123.5	3.8
146.4	3.6	176.9	2.7	191.9	2.5	136.0	2.6	97.8	3.3
140.5	4.2	145.7	2.5	196.8	2.3	117.1	2.8	153.8	3.9
198.0	4.5	121.9	2.1	203.6	3.2	137.3	2.9	92.2	2.9
119.5	4.2	109.9	2.0	191.5	3.4	70.8	3.4	145.7	3.7
147.1	3.6	105.1	2.0	127.7	3.9	88.4	2.8	115.9	3.8
92.2	3.4	272.0	2.3	302.2	3.1	219.7	3.6	136.5	2.7
198.6	4.7	177.3	3.2	115.4	3.6	63.8	3.3	113.2	3.5
211.6	4.9	173.0	2.9	114.2	3.9	160.9	3.1	64.0	3.4
90.2	4.5	172.5	2.6	139.2	3.0	101.7	3.5	122.8	3.2
100.1	3.6	146.7	2.7	109.6	3.7	145.9	4.0	168.5	3.2
151.7	4.0	122.1	2.1	160.8	3.7	113.6	4.0	112.9	3.9
184.3	4.0	259.4	3.3	97.8	3.8	146.4	3.4	114.0	3.4
112.3	4.1	173.8	3.0	90.2	3.6	139.6	2.9	143.9	3.3
112.8	4.3	78.9	2.4	74.4	4.0	186.0	3.0	109.4	3.7
155.5	4.5	122.9	1.9	133.2	3.3	154.7	2.9	101.9	3.5
198.3	4.2	148.0	2.5	73.9	3.8	103.3	3.7	72.1	3.3
107.2	3.7	100.8	2.3	90.2	3.3	78.7	3.6	147.9	2.8

138.6	4.1	141.6	3.3	232.0	2.7	217.9	3.5	200.4	3.3
130.4	3.7	108.7	3.1	64.0	3.5	142.6	2.8	137.3	4.0
95.8	4.5	237.8	2.8	64.0	3.4	156.6	3.1	145.0	3.8
161.2	4.0	260.6	2.6	151.6	3.6	117.2	3.8	129.8	3.6
112.7	3.5	138.1	2.7	120.0	3.5	122.8	2.6	86.9	3.8
104.6	4.3	58.6	2.8	195.3	3.2	86.2	2.8	155.5	3.5
170.3	3.9	118.9	2.8	135.6	2.5	130.3	3.9	86.3	3.8
131.7	3.5	101.2	2.7	73.0	3.0	129.0	3.3	-------	-------

Table 6.3 - AFM measurements of length (L_r) and diameter (d_r) of individual CTNW rods.

L_r	d_r	L_r	d_r	L_r	d_r	L_r	d_r	L_r	d_r
317.5	7.5	296.9	8.1	339.2	9.0	267.7	5.2	351.1	6.8
387.2	7.4	192.2	5.7	245.5	4.8	289.9	5.7	319.2	4.2
316.9	5.3	233.5	5.5	531.3	9.0	567.9	6.9	226.0	5.3
254.3	6.0	246.2	6.0	432.1	4.9	235.5	6.6	798.7	4.6
169.7	4.8	394.2	5.5	390.3	5.7	220.7	6.2	394.2	4.7
342.2	6.6	237.7	6.2	370.7	6.6	455.2	8.1	271.8	4.8
128.1	6.1	465.2	4.9	277.5	4.8	282.7	4.5	322.1	5.0
270.0	7.3	330.6	3.2	333.6	4.5	348.9	4.0	355.8	3.9
415.4	8.1	279.5	7.5	365.1	6.8	322.0	6.7	414.0	6.4
111.5	7.9	455.3	6.4	167.3	5.4	291.3	7.6	186.3	4.5
289.1	6.4	526.9	5.7	252.7	7.0	418.0	6.3	145.3	5.7
265.1	6.3	534.1	7.3	338.8	7.8	183.6	5.8	330.4	5.4
137.9	6.6	200.3	5.7	231.5	5.4	473.3	6.9	406.4	5.3
176.3	7.3	138.0	6.6	184.3	4.6	214.0	6.0	255.1	4.6
231.7	4.6	111.5	6.0	249.1	5.9	191.2	3.4	135.9	6.4
363.7	7.3	161.4	6.7	407.3	6.0	189.9	5.2	283.5	6.2
379.6	9.5	267.2	6.3	268.6	4.6	436.6	3.9	145.6	4.9
277.4	5.9	142.4	5.3	408.1	4.9	429.7	5.8	262.6	5.9
212.0	6.5	233.7	8.6	141.2	5.2	328.9	7.1	715.2	5.0
500.7	7.5	298.4	8.3	433.5	4.4	174.1	4.1	157.0	4.5
237.1	3.6	292.6	8.2	197.4	4.1	146.4	4.3	330.2	5.6

689.7	4.7	328.7	7.9	232.7	5.3	257.3	5.9	-------	-------

6.4 “Hand-draw 3D printing” of CNC and CTNW

As described previously, several experiments were performed in order to determine the conditions which was possible to “hand-draw 3D print” a structure with high robustness. In Figure 6.3 are presented photos of all experiments made using CNC:alginate bioink and described in the results section.

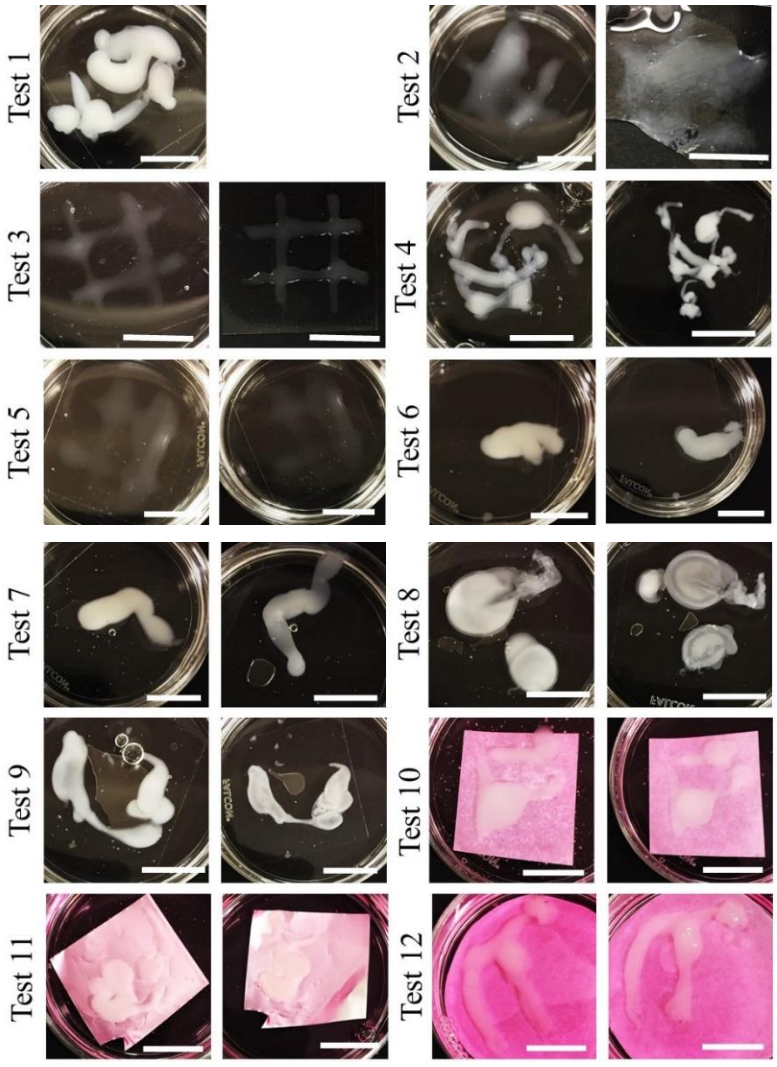

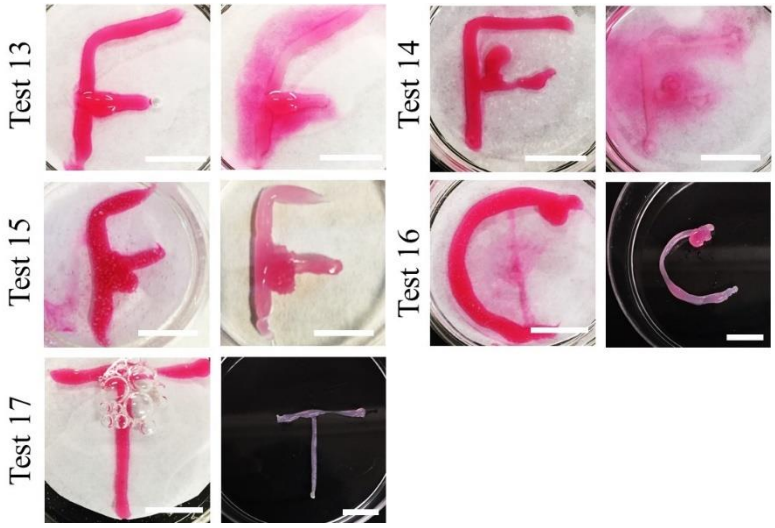

Figure 6.3 – Photos of all experimental tests of 3D printing by using CNC:alginate bioink. In each set of images the first was taken immediately after printing and the second after air drying. Scale bars: 1 cm.

The tests of CTNW:alginate bioink were performed as a continuation of CNC bioink and are presented in Figure 6.4. The "A" tests were performed using a PVA 10 % wt. $CaCl_2$ 25 mM cross-linking solution, while in the "B" tests PVA 10 % wt., $CaCl_2$ 50 mM mixture was used as cross-linking solution. The tests 1, 2, 3 and 4 were preformed using 4:1, 3.5:1, 3:1 and 2.5:1 CTNW:alginate volume ratios, respectively.

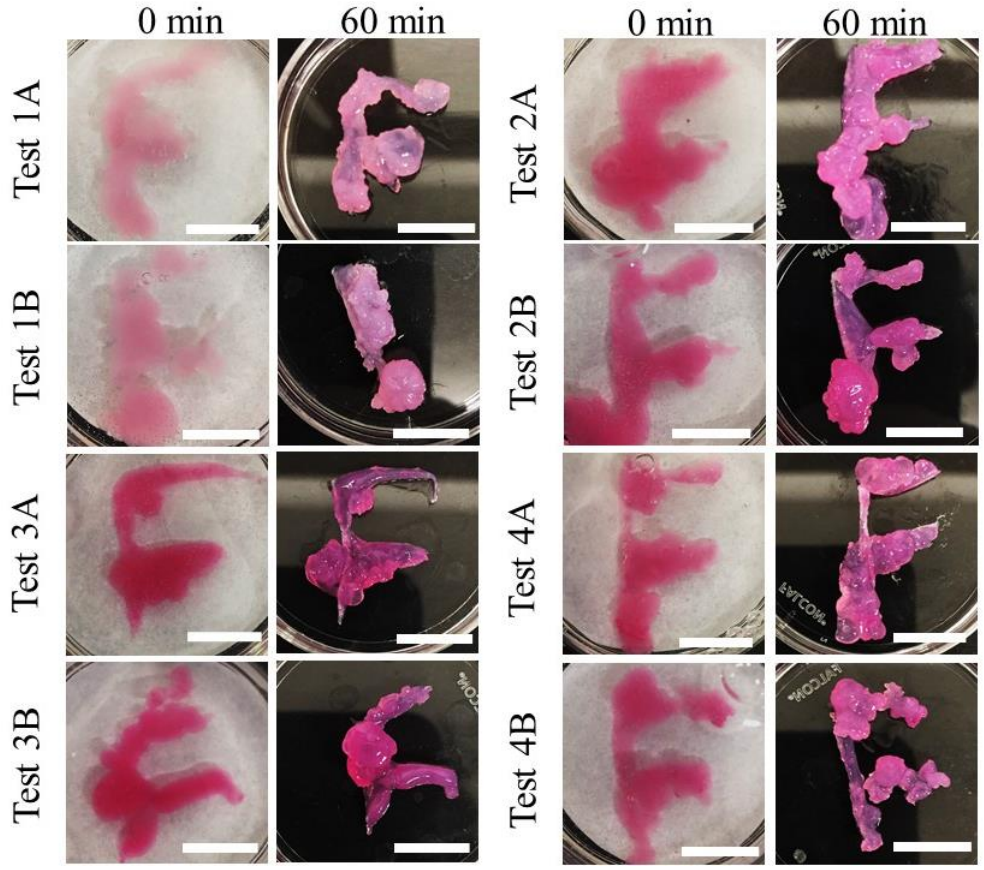

Figure 6.4 – Photos of all experiments made using CTNW (1.9 % wt.):alginate bioink. 0 minutes column is right after the extrusion of the ink, while 60 minutes column is after cross-linking for 60 minutes, wash with ultrapure water and dried with filter paper. Scale bar: 1cm.

The designing of the structures was made at Tinkercad™ and the designed structured are presented in Figure 6.5. The three structures designs have 6×7×3 mm of length, width and height respectively.

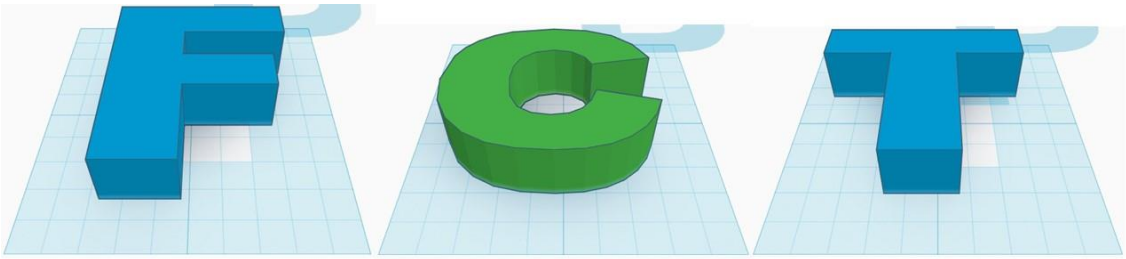

Figure 6.5 – Preview of the designed structures in Tinkercad™. Grid: 10×10 mm.